Published online 11 January 2023

Nucleic Acids Research, 2023, Vol. 51, No. 3 ***1375–1392***
https://doi.org/10.1093/nar/gkac1245

The formation of HuR/YB1 complex is required for the stabilization of target mRNA to promote myogenesis

Brenda Janice Sánchez[1,2,3,4], Souad Mubaid[3,4], Sandrine Busque[3,4], Yossef Lopez de los Santos[2], Kholoud Ashour[3,4], Jason Sadek[3,4], Xian Jin Lian[3,4], Shahryar Khattak[1,2], Sergio Di Marco[1,2,3,4] and Imed-Eddine Gallouzi[1,2,3,4,*]

[1]KAUST Smart-Health Initiative King Abdullah University of Science and Technology (KAUST), Jeddah, Saudi Arabia, [2]KAUST Biological Environmental Science and Engineering (BESE) Division, King Abdullah University of Science and Technology (KAUST), Jeddah, Saudi Arabia, [3]Dept. of Biochemistry, McGill University, 3655 Promenade Sir William Osler, Montreal, QC H3G1Y6, Canada and [4]Rosalind & Morris Goodman Cancer Institute, McGill University, 1160 Pine Avenue, Montreal, QC H3A1A3, Canada

Received November 24, 2022; Editorial Decision November 30, 2022; Accepted December 14, 2022

ABSTRACT

mRNA stability is the mechanism by which cells protect transcripts allowing their expression to execute various functions that affect cell metabolism and fate. It is well-established that RNA binding proteins (RBPs) such as HuR use their ability to stabilize mRNA targets to modulate vital processes such as muscle fiber formation (myogenesis). However, the machinery and the mechanisms regulating mRNA stabilization are still elusive. Here, we identified Y-Box binding protein 1 (YB1) as an indispensable HuR binding partner for mRNA stabilization and promotion of myogenesis. Both HuR and YB1 bind to 409 common mRNA targets, 147 of which contain a U-rich consensus motif in their 3′ untranslated region (3′UTR) that can also be found in mRNA targets in other cell systems. YB1 and HuR form a heterodimer that associates with the U-rich consensus motif to stabilize key promyogenic mRNAs. The formation of this complex involves a small domain in HuR (227–234) that if mutated prevents HuR from reestablishing myogenesis in siHuR-treated muscle cells. Together our data uncover that YB1 is a key player in HuR-mediated stabilization of pro-myogenic mRNAs and provide the first indication that the mRNA stability mechanism is as complex as other key cellular processes such as mRNA decay and translation.

INTRODUCTION

Mammalian adult skeletal muscle tissue is composed of bundles of fibers derived from the fusion of several mononucleated muscle pre-cursor cells (myoblasts) (1–3). The integrity of muscle tissue is vital for an organism to ensure its basic functions, such as locomotor activity, postural behavior, and breathing. Therefore, it is not surprising that myogenesis (the process of muscle formation and regeneration) is tightly regulated and highly conserved in all mammals (4–9). Myogenesis is activated during embryogenesis, leading to the formation of skeletal muscle tissue, as well as in response to injury, to allow the regeneration of damaged muscle fibers (1,2,4,7). The myogenic process involves the sequential activation of a specific set of transcription factors known as myogenic regulatory factors (MRFs), which promote muscle cell differentiation through the induction of a muscle-specific transcriptional program during the various stages of this process (2,5,6,8,9). These MRFs consist of myogenic differentiation antigen (MyoD), myogenin (Myog), myogenic factor 5 (Myf5) and myogenic factor 6 (MRF4). It is well established that high levels of these MRFs must be maintained throughout the differentiation process in order to ensure the proper development and integrity of muscle (2–10). While it is well-accepted that transcriptional induction of genes encoding these MRF represents a critical regulatory step during myogenesis, work from several groups has established that transcription alone is not sufficient to maintain the high expression levels of MRFs needed during this process (11–14).

The regulation of gene expression at the posttranscriptional level has been previously shown to play a critical role in modulating muscle fiber formation (12–15). This dynamic level of regulation involves many steps in the maturation of mRNA including splicing, stability of the mRNA transcript, cellular movement, and translation of the mRNA into protein (16–18). RNA-binding proteins (RBPs) are one of the key posttranscriptional regulatory trans-acting factors that help mRNAs undergo these regulatory events in various cells including muscle (16–18). We

*To whom correspondence should be addressed. Tel: +966 12 808 2354; Email: gallouzi.imed@kaust.edu.sa

and others have shown that the RBP HuR, a well characterized posttranscriptional regulator, plays a key role in promoting myogenesis (12–14,19–27)The mechanisms by which HuR performs its pro-myogenic function during the various stages of myogenesis are unique and sometimes opposing. Indeed, during the early stages of this process, HuR promotes the expression of the alarmin HMGB1 by preventing miR-1192-mediated translation inhibition of its mRNA (26). Simultaneously, HuR collaborates with the RBP KSRP to reduce the expression of the nucleophosmin (NPM) protein by destabilizing its mRNA (27). We, additionally, have shown that, during the pre-terminal stage of the differentiation process, HuR executes yet another important function by stabilizing the *MyoD* and *Myog* mRNAs (20,22), the mechanism of which is still unknown.

Over the last three decades major efforts have been made to identify the machineries (trans-acting factors, cis-elements, etc.) and delineate the mechanisms modulating mRNA splicing, transport, decay and translation (28–32) However, our current understanding of mRNA stabilization mechanisms is limited. Indeed, the majority of the studies have associated the binding of a single RBP, such as HuR, to a specific *cis*-element as being sufficient to stabilize a given mRNA protecting it from decay (20,21,33–35). Therefore, in order to address this gap of knowledge, the objective of this study is to identify and characterize the protein network and *cis*-element (s) required for HuR-mediated stabilization of target mRNAs during myogenesis.

Here, we identified the multifunctional DNA/RNA-binding protein YB1 (36–38) as a novel HuR binding partner during the myogenic process. We established that YB1, similarly to HuR, is essential for the formation of muscle fibers due, in part, to the stabilization of common pro-myogenic mRNA targets. Bioinformatic analyses uncovered a consensus HuR/YB1 stabilizing U-rich motif in the 3′UTR of common mRNAs. Additionally, our data show that the prevalence of this HuR/YB1 binding motif extends beyond muscle cells. We also show that the HuR/YB1 complex is required for the stabilization of mRNA targets during muscle fiber formation. Taken together our results provide evidence that HuR and YB1 may constitute a stabilizing complex that mediates the fine tuning of mRNA stabilizing mechanisms that regulate the outcome of cellular programs such as myogenesis.

MATERIALS AND METHODS

Plasmid construction

To generate the GST-YB1 plasmid, the mouse YB1 coding sequence was amplified by PCR and cloned into the pGEX-6P-1 plasmid (GE Healthcare). GFP-HuR was prepared by PCR using the GST-HuR (39) plasmid as a template. The PCR fragments were then cloned into the pAcGFP1-C1 vector (BD Biosciences). GFP-Myog was prepared by PCR amplification of the mouse Myog coding sequence and 3′UTR which was the cloned into the pAcGFP1-C1 vector (BD Biosciences) (20). To generate the pRL-*Myog*-3′UTR plasmid, the full-length 3′-UTR of mouse *Myog* was amplified by PCR and cloned into the pRL-SV40 plasmid (Promega). pRL-*Myog*-3′UTR or GFP-Myog mutants were generated by Norclone Biotech Laboratories, London, ON, Canada. Full sequence is detailed in Supplementary Table S10.

Cell culture

C2C12 cells (ATCC, Manassas, VA, USA) were grown and maintained in Dulbecco's modified eagle medium (DMEM, Invitrogen) containing 20% fetal bovine serum (Invitrogen), and 1% penicillin/streptomycin antibiotics, following the manufacturer's instructions (Invitrogen). Differentiation was induced when the cells reached 100% confluency on plates previously coated with 0.1% gelatin (Day 0). To induce differentiation, growth media was replaced with differentiation media containing DMEM, 2% horse serum, and 1% penicillin/streptomycin antibiotics.

Transfection

The transfection of siRNA into C2C12 cells was performed as previously described (20). Briefly, the transfection with siYB1, siHuR, siCtl or mock (transfection buffer only) was performed when cells were 20–30% confluent. The transfection treatment was repeated 24 h later when cells were 50–60% confluent. 6–8 h after the second transfection, two wells (with the same siRNA treatment) were combined into one by trypsinizing the cells from one well and transferring them to the corresponding well on the second plate. All siRNA duplexes were used at a final concentration of 60nM. For DNA plasmid transfections C2C12 cells, at 60–70% confluency, were transfected in six-well plates with 1.5 μg of plasmid DNA. jetPRIME® (Polyplus) transfection reagent was used for all transfections following the manufacturer's instructions. siRNA sequences are provided in Supplementary Table S10.

Preparation of cell extracts and immunoblotting

Cell extracts were prepared by incubating undifferentiated or differentiated C2C12 cells on ice for 15 min with lysis buffer (50 mM HEPES pH 7.0, 150 mM NaCl, 10% glycerol, 1% Triton, 10 mM pyrophosphate sodium, 100 mM NaF, 1 mM EGTA, 1.5 mM $MgCl_2$, 1× protease inhibitor (Roche)). The lysed cells were then centrifuged at 12 000 rpm for 15 min at 4°C in order to remove cell debris. The extracts were then run on an SDS-PAGE gel and transferred to nitrocellulose membranes (BioRad). Finally, the samples were analyzed by western blotting with antibodies against HuR (3A2) (39), 1:10 000), YB1 (ab12148 Abcam, 1:1000), Myog (F5D, Developmental studies Hybridoma Bank, 1:250), GFP (Takara, 1:1000), or α-tubulin (Developmental studies Hybridoma Bank, 1:1000) as loading control.

Immunofluorescence

Immunofluorescence was performed as previously describe (20). Briefly, cells were rinsed twice in PBS, fixed in 3% phosphate-buffered paraformaldehyde (Sigma), and permeabilized in PBS-goat serum with 0.5% Triton. After permeabilization, cells were incubated with primary antibodies against the RBPs HuR (1:1000) and YB1 (1:500) or against

markers of muscle cell differentiation, Myosin Heavy Chain (MyHC) (1:1000) and Myoglobin (1:250), in 1% normal goat serum/PBS at room temperature for 1 hr. The cells were then incubated with goat anti-mouse or goat anti-rabbit secondary antibodies (Alexa Fluor® 488, 594) and stained with DAPI (4′, 6-diamidino-2-phenylindole) to visualize the nucleus. A Zeiss Axiovision 3.1 microscope was used to observe the cells using a 40× oil objective, and an Axiocam HR (Zeiss) digital camera was used for immunofluorescence photography.

Fusion index

The fusion index indicating the efficiency of C2C12 differentiation was determined by calculating the number of nuclei in each microscopic field in relation to the number of nuclei in myotubes in the same field as previously described (20). Fusion index on GFP transfected cells was determined by calculating the number of GFP-tagged nuclei in each microscopic field in relation to the number of GFP-tagged nuclei in myotubes in the same field as previously described.

RNA extraction and actinomycin D pulse-chase experiments

mRNA stability was assessed by treating the cells with the RNA polymerase II inhibitor, actinomycin D (ActD) (5 μg/ml), for 0, 2, 4 and 6 hours. Total RNA was isolated at the indicated periods of time using Trizol reagent (Invitrogen) according to the manufacturer's instructions.

RT-qPCR

1μg of total RNA was reverse transcribed using the M-MuLV RT system (New England BioLab). A 1:80 dilution of cDNA was then used to detect mRNA levels using SsoFast™ EvaGreen® Supermix (Bio-Rad). Expression was standardized using *GAPDH or RPL32* as a reference, and relative levels of expression were quantified by calculating $2^{-\Delta\Delta C}{}_T$, where $\Delta\Delta C_T$ is the difference in C_T (cycle number) at which the amount of amplified target reaches a fixed threshold between target and reference. In the case of immunoprecipitated samples a 1:20 dilution was used. Primer sequences can be found in Supplementary Table S10.

Immunoprecipitation (co-IP & RIP)

15 μl of anti-YB1, anti-HuR or IgG antibodies were incubated with 60μl of protein A-Sepharose slurry beads (washed and equilibrated in cell lysis buffer) for 4 h at 4°C. Beads were washed three times with cell lysis buffer and incubated with 500 μg of cell extracts overnight at 4°C. Beads were then washed again three times with cell lysis buffer and co-immunoprecipitated proteins and/or RNA was then eluted and processed for analysis. When indicated, cell extracts were digested for 30 min at 37°C with RNase A (100 μg/ml) prior to the immunoprecipitation.

RNA electrophoretic mobility shift assays (REMSA)

Myog cRNA probes G/URE1 and G/URE2 were generated using sense and antisense oligonucleotides complementary to these regions which were directly annealed. probe G/URE-3 was generated by PCR amplification using a forward primer fused to the T7 promoter as well as the pEMSV-Myog plasmid (kindly Supplied by Dr A. Lassar, at Harvard Medical School) as template. Probes were then used for *in vitro* transcription reactions using a T7 RNA polymerase (Promega). 500 ng of purified protein (glutathione S-transferase (GST), GST-YB1 or GST-HuR was incubated with 100,000 cpm of [α-^{32}P] -UTP-labeled cRNAs in a total volume of 20 μl EBMK buffer (25 mM HEPES, pH 7.6, 1.5 mM KCl, 5 mM $MgCl_2$, 75 mM NaCl, 6% sucrose and protease inhibitors) at room temperature for 15 min. Two microliters of a 50 mg/ml heparin sulfate stock solution were then added to the reaction mixture for an additional 15 min at room temperature to prevent nonspecific protein-RNA binding. Finally, samples were loaded on a non-denaturing 4% polyacrylamide gel containing 0.05% NP-40 and run for 2 h at 180 V. Gels were then fix in 7% acetic acid/10% ethanol, dried and exposed overnight at −80°C. Primer sequences can be found in Supplementary Table S10.

Luciferase expression/activity

Renilla luciferase mRNA steady state levels were determined by RT-qPCR using primers specific for Rluc. Primer sequences can be found in Supplementary Table S10. Luciferase activity was furthermore measured using a Renilla luciferase assay system (Promega) following the manufacturer's instructions.

mRNA sequencing (RNA-seq)

RNA was isolated from IP experiments (using anti-YB1, anti-HuR or IgG antibodies) performed on C2C12 total cell extract collected at day 2 of differentiation, using TRIzol reagent (Invitrogen). RNA samples were assessed for quantity and quality using a NanoDrop UV spectrophotometer (Thermo Fisher Scientific Inc), and a Bioanalyser (Agilent Technology Inc). The three RNA-seq libraries (anti-IgG, anti-YB1 and anti-HuR) were sequenced on the Illumina NextSeq 500 platform at the Institute for Research in Immunology and Cancer (IRIC) Genomics Core Facility, University of Montreal, to produce over 37 million, 100 nucleotide paired-end reads per sample. The reads were then trimmed for sequencing adapters and aligned to the reference mouse genome version mm10 (GRCm38) using Tophat version 2.0.10. (40) Gene quantification was performed on the mapped sequences using the htseq-count software version 0.6.1. (41) All the raw sequences are deposited on the Gene Expression Omnibus (GEO) database repository from The National Center for Biotechnology Information (NCBI) under the accession number GSE178419.

Mass spectrometry

Proteins immunoprecipitated with IgG (negative control) or HuR (using antibodies against HuR or IgG) from extracts obtained on 2-day post-induction of muscle cell differentiation were analyzed by mass spectrometry at the Centre de

recherche du CHU de Québec. Proteins that showed enrichment in the anti-HuR samples but not the anti-IgG controls were considered for analysis.

Gene ontology analysis

GO analysis using DAVID 6.8 (42,43)was performed on gene targets identified by mass spectrometry and RIP-seq. Gene targets were evaluated for their Biological Processes (BP) and/or Cellular Compartment (CC). The EASE Score, a modified Fisher exact *P*-value, was used for gene-enrichment analysis.

GeneMANIA

GeneMANIA web interface is available at http://www.genemania.org (44). The input to GeneMANIA consisted of the RBPs found to be associated to HuR in our IP experiments (Figure 1C, Supplementary Tables S1 and S2). The GeneMANIA algorithm then extended the initial query protein list to 36 by predicting the involvement of 20 additional related proteins (Supplementary Table S2). Stripe nodes represent the queried genes and non-stripe nodes represent mediated protein for interactions (predicted by GeneMANIA). Physical interaction analysis is displayed as pink lines, co-localization analysis as violet lines. Line thickness represents interaction strength. Molecular functions are shown by color triangles inside each node. Proteins are identified by their gene name.

Identification of consensus motif

The MEME software was used to discover ungapped sequence motifs representing protein binding sites in the 3′UTR of HuR and YB1 common mRNA targets. The 3′UTRs sequences were obtained from the NCBI nucleotide database by selecting the sequence between the end of the coding region and the end of the mRNA in a FASTA format. MEME suite identified sequence patterns in the list of sequences as previously describe (45). The occurrence of the motif in individual mRNAs was available from the output data of the MEME analysis.

Bioinformatical analysis of existing PAR-CLIP (photoactivatable ribonucleoside enhanced cross-linking and immunoprecipitation)

Bioinformatical Analysis of existing PAR-CLIP (46) data (deposited in the Gene Expression Omnibus database under accession number GSE133620) was performed by the Canadian Centre for Computational Genomics (C3G). The peaks regions for these two proteins were obtained from the GEO Datasets (GSM3913321, GSM3913322, GSM3913323, GSM3913324). Replicates were merged to create consensus peaks using BEDtools (47). The regions where YB1 and HuR binding regions overlapped were then obtained. Homer was used for genomic region annotation (48). The occurrence of the motif identified in the MEME (described above) in the regions of co-occurring binding was performed by FIMO (45)

Surface plasmon resonance (SPR)

SPR analysis were performed as a service by the CERMO-FC platform at the Universite du Quebec a Montreal. Briefly, affinity measurement and kinetic analysis of HuR and YB1 binding to the cDNA probes was performed by injecting different known concentrations of cDNA probes (from 0 to 2000 nM) onto immobilized GST-recombinant proteins. For immobilization, carboxymethyl dextran-coated CM5 sensor chips were used with amine coupling chemistry. Different concentrations of cDNA probes were injected onto the capture recombinant proteins at a flow rate of 30 μl/min for 400 s to check the kinetics of association. Biosensor matrices were regenerated after each run using glycine–HCl buffer at pH 2.0. for 30 s at 30 μl/min and then 10 mM NaOH for 30s at 30 μl/min, stabilization period of 600 s. Biacore T200 evaluation software (version 1.0) was used to determine k_d (dissociation constant) and ka (association constant) values. K_D (equilibrium constant) values were calculated from the obtained k_d and k_a values.

Generation of the HuR and YB1 protein models

Protein structure models of HuR and YB1 were obtained as a result of an intensive process of calculation, comparison and scoring of the best protein models generated by seven independent modeling processes. A homology modeling was performed to generate the HuR and YB1 protein models. PSI-Blast and HHblits algorithms were used to identify the best structural template candidates for modeling for both targets (49,50). To overcome the intrinsic limitations of the modeling process the outputs of seven independent systems were compared: Galaxy (51), HHPRED-modeller (52), I-Tasser (53), Phyre2 (54), Robetta 55–57, SWISS-MODEL (58) and YASARA modeling package (59). The best computed models for each system were independently ranked and selected by their own scoring functions for further validation. Additional model validation included evaluation of the best atomic solvation and molecular packing by SolVX (60), structural validation by calpha geometry (61), statistical error evaluation by model regions calculated based on nonbonded interactions between different atom types relative to a curated database of highly refined structures (62), determination of model compatibility with its own residue sequence based on local environment (63), stereochemical quality of the protein structure (64), and composite scoring function for homology model quality estimation (65).

Molecular docking simulation of the HuR-YB1 protein-protein complex

To obtain the most energetically stable versions of both protein conformations (i.e. the HuR and YB1 structures that exhibited the lowest energy thresholds), energy minimization preprocessing of the structures was performed with the YASARA force field (59). To overcome simulation biases and limitations of the protocols used to simulate protein-protein binding phenomena, six independent systems Frodock (66), GalxyTongDock (67), HDOCK (68),

ClusPro (69), Patchdock (70) and SwarmDock (71) were used. Each of these options explores the solution set in its own way, showing different strengths and pitfalls. Since the best complexes emerged from such heterogeneity of search systems, the combination of results leads to better cover the drawback of relying on the use of a single protocol. At least the top 10 ranked models per system were selected (i.e. at least 60 protein–protein complexes were generated). Finally, the three best global complex models were further refined using the RosettaDock protocol (72). The standard RosettaDock protocol was applied to locally refine the protein-protein complexes by selecting the models with the lowest energy by repositioning side chains, loops, and moderately adjusting the protein backbone. As a result of RosettaDock refinement, the top ranked model from a set of 1000 models (i.e. the protein complex with the lowest energy) was selected. All molecular graphical analyses and figures were performed and generated with UCSF Chimera version 1.1 (73).

Molecular docking simulation of the HuR-YB1-*Myog* ternary complex

The ternary complex was obtained using the top ranked models of the HuR-YB1 complexes with the RNA structures predicted by the FARFAR2 tool (74). Briefly, the *Myog* 3′UTR structure was obtained by using the FARFAR2 tool that is based on the ROSSETA protocol for molecular structural prediction. The IPknot tool was used for the prediction of the *Myog* RNA secondary structures that FARFAR2 used as input (75). A total of 10 000 solutions for the RNA molecule were calculated, classified, clustered and scored according to FARFAR2 default parameters. The most stable *Myog* RNA conformation of the most represented cluster (group of structures with very similar RNA folding) was further explored by molecular docking with the HuR-YB1 protein complex by HDOCK (76). Our simulation protocol considered protein-protein docking as the first logical step followed by the protein-RNA complex docking process. Of the three top-ranked ternary complexes, our final model was selected based on three key features. (i) The ternary model must allow interaction of YB1 with the G/URE2 of *Myog* (amino acids 65–116). (ii) At least one of the three HuR RNA recognition motifs (RRM) must be able to independently bind with the G/URE-2 of *Myog*. (iii) The protein–protein interface of the HuR–YB1 complex would have to be uncompromised by a potentially competing RNA interaction to establish a new RNA-protein complex.

Statistical analyses

All results are from three independent experiments unless stated otherwise in the figure legends. All values are reported as mean ± standard error of the mean (SEM). Significance of the difference between two group means was assessed by unpaired *t*-test for normally distributed variables. *P*-values of <0.05 were considered significant.

RESULTS

YB1 is a novel HuR protein ligand that is required for muscle fiber formation

To identify novel protein ligands that interact with HuR during the later stages of muscle cell differentiation we immunoprecipitated (IP) HuR from C2C12 cell extracts collected at day 2 (post-induction of the differentiation process) (Figure 1A). Mass spectrometry analysis of the HuR-bound proteins, under these conditions, identified 41 putative protein ligands of HuR (Supplementary Table S1). Gene Ontology (GO) classification of HuR protein ligands by molecular function (Figure 1B) and cellular compartment (Supplementary Figure S1A) revealed that these ligands are most commonly RBPs, as well as proteins localized in ribonucleoprotein complexes. The 15 RBPs found to be associated to HuR in muscle cells (Figure 1C, Supplementary Table S1) were then used to generate a protein-protein interaction network to further understand the relationship between HuR and these ligands (Figure 1D, Supplementary Table S2). Our analysis revealed that among the bound RBPs, YB1 shares the most molecular functions with HuR (mRNA stabilization, mRNA binding, regulation of mRNA stability) (Figure 1D). YB1 was previously shown to mediate the maturation of Neuro Muscular Junctions (77,78) as well as to regulate the transcription of the *myod* gene in muscle cells (37,38). Therefore, we sought to determine if the interaction of YB1 with HuR plays an important role in regulating the function of HuR during myogenesis. We first validated our mass spectrometry results by performing reciprocal IP experiments using an anti-HuR antibody (Figure 1E) or anti-YB1 antibody (Supplementary Figure S1B) on C2C12 muscle cells collected 2 days post-induction of differentiation. Our results further demonstrated that YB1 and HuR associate with each other during the pre-terminal stage of muscle fiber formation (2 days post-induction of differentiation) (Supplementary Figure S1C). We next assessed if the interaction between HuR and YB1 occurred in an RNA dependent or independent manner. By performing the IP experiment using the anti-HuR antibody and C2C12 cell extracts treated with or without 100 μg/ml RNAse-A we observed that this association indeed occurs in an RNA-independent manner (Figure 1E). Western blot (WB) experiments using total cell extracts from differentiating muscle cells demonstrated that neither HuR nor YB1 expression is altered during myogenesis (Supplementary Figure S1D). Hence, their interaction during the pre-terminal phase was not the result of an increased expression of HuR or YB1.

It is well established that the cytoplasmic accumulation of HuR during muscle cell differentiation directly correlates with its function in regulating the expression of its promyogenic targets(19,20,22). The fact that similarly to HuR, YB1 is also known to shuttle between the nucleus and the cytoplasm (38,79,80) raises the possibility of a direct relation between YB1 localization in muscle cells and its association to HuR. To investigate this possibility, we visualized the cellular localization of HuR and YB1 during muscle fiber formation. Contrary to HuR, which is localized in the

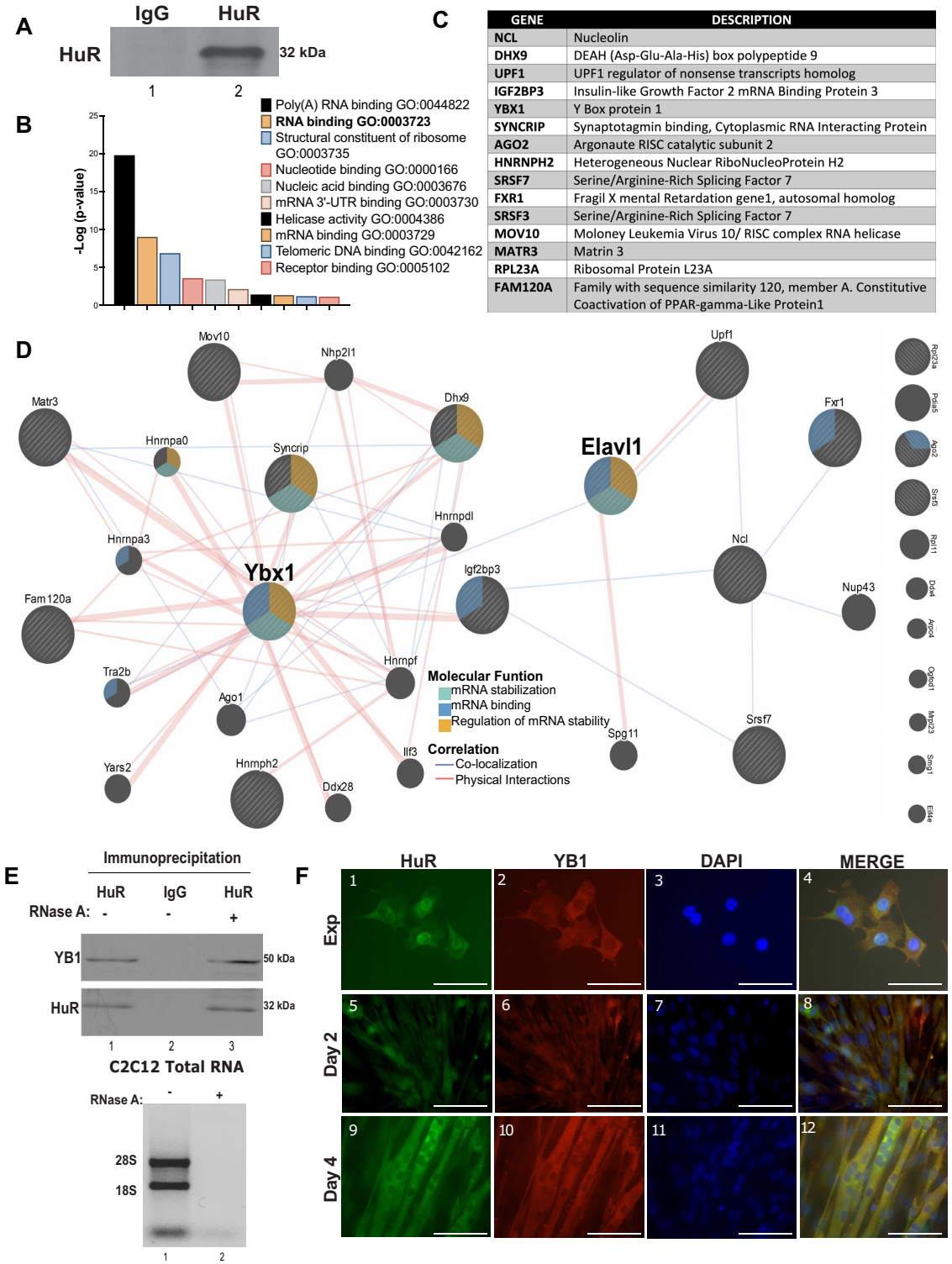

Figure 1. YB1 is a novel HuR protein partner in pre-terminal myotubes. (**A**) IP experiments were performed on C2C12 cell lysates (harvested 2 days post-induction of differentiation) using a monoclonal HuR antibody (3A2) or IgG as control. IP samples were analyzed by western blot using an anti-HuR antibody. (**B**) Protein partners of HuR from the IP shown in A were identified by mass spectrometry analysis (from N = 1 experiment). GO-analysis was conducted using DAVID v6.8Ⓡ to classify HuR putative protein partners based on molecular functions. The top 10 GO-terms enriched, as analyzed by DAVID v6.8Ⓡ, are shown. (**C**) List of RBPs identified by GO analysis. (**D**) GeneMANIA interaction network of HuR putative protein ligand in muscle. (**E**) Top; IP experiments were performed on C2C12 cell lysates collected on D2 post-induction of differentiation treated or not with RNase A using a monoclonal HuR antibody (3A2) or IgG as a control; IP samples were analyzed by WB using anti-YB1 or -HuR antibodies. **Bottom;** Agarose gel demonstrating the efficiency of RNA degradation in cell extracts digested for 30 min at 37°C with RNase A (100 μg/ml). (**F**) IF pictures showing the cellular localization of YB1 and HuR in exponentially growing C2C12 myoblasts (Exp), and C2C12 myotubes at 2- and 4-day post-induction of differentiation. Images of a single representative field are shown. Bars 100 μm.

nucleus in myoblasts and localizes to the cytoplasm upon induction of muscle cell differentiation (Figure 1F, panels 1, 5, 9) (22), our immunofluorescence (IF) experiments revealed that YB1 is primary found in the cytoplasm of myoblasts and that there is no change in its localization during myogenesis (Figure 1F, panels 2, 6, 10). Our data therefore indicate that HuR and YB1 interact with each other during the pre-terminal stage, at a time when they are both localized in the cytoplasm of myotubes.

We next assessed whether YB1, similarly to HuR, plays an important role in regulating the myogenic process. We first knocked down YB1 in myoblasts using an siRNA that specifically targets the *Ybx1* gene (siYB1) (Figure 2A) We observed that while the knockdown of YB1 in C2C12 cells did not affect cell viability (Supplementary Figure S2A) it significantly reduced (>10-fold) the efficiency of muscle cell differentiation as determined by phase contrast (Figure 2B) and immunofluorescence (IF) experiments (Figure 2C). Next, we evaluated whether overexpression of HuR which, on its own, enhances muscle fiber formation (23,24), could rescue the differentiation phenotype of siYB1 treated cells. As expected, GFP-HuR expression in siCtl treated myoblasts resulted in the improved differentiation of these cells (Figure 2D and E, panels 2, 6). However, this effect was prevented by the knockdown of YB1 (Figure 2D and E, panels 4, 8). Importantly, exogenous expression of HuR had no effect on endogenous YB1 or HuR protein levels (Figure 2D and Supplementary Figure S2B). Therefore, these observations suggest that YB1 is required for the promyogenic function of HuR.

YB1 and HuR bind to common target mRNAs via a consensus U-rich motif in the 3′UTR

In order to investigate if HuR and YB1 function together during myogenesis to affect the expression of common promyogenic mRNA targets as a first step, we performed RNA immunoprecipitation (RNA-IP) experiments (using anti-HuR and anti-YB1 antibodies) coupled to RNA sequencing experiments (RIP-seq) on C2C12 cell extracts collected at day 2 post-induction of differentiation. We determined that, in muscle cells, HuR and YB1 associate with 1513 and 1103 mRNA transcripts respectively (Supplementary Table S3). Comparison of both RIP-seq datasets identified that HuR and YB1 interact with 409 common mRNA targets (Figure 3A, Supplementary Table S4). It is well established that both YB1 and HuR modulate the expression of target mRNAs by directly interacting with regulatory elements located in their 3′UTRs (24,36). Therefore, to characterize YB1/HuR binding to its target transcripts, we identified potential binding sites in the 3′UTRs of the 409 shared mRNA targets using the motif analysis software MEME Suite (45). Motif discovery analysis revealed several potential consensus motifs that interacted with the HuR/YB1 complex (Supplementary Figure S3A). Of these, the one with the highest probability of being a binding site was detected in 147 of the 409 shared target transcripts (Figure 3B, Supplementary Table S5).

Both HuR and YB1 were previously shown by Chen *etal*. to bind common mRNA targets in human urothelial cells (46). We, therefore, proceeded to re-analyze the PAR-CLIP data sets for HuR and YB1 (presented in that study) in order to assess the commonality of our consensus motif beyond the myogenic process. Analysis of these data demonstrated that while YB1 associates with 25 383 binding sites distributed over 7666 genes, HuR interacts with 40 150 binding sites distributed over 10102 genes (Figure 3C). In both cases, the majority of these binding sites were located within the gene body thus supporting a putative role of these RBPs in the posttranscriptional regulation of these genes (Figure 3D). Peak size distribution was similar amongst both data sets (Supplementary Figure S3B). Comparative analysis of the HuR and YB1 datasets further revealed that both interact with 5584 common overlapping binding sites. Interestingly, almost half of these shared binding sites (2507 sites) were localized within the 3′UTR of 1370 genes (Figure 3E, Supplementary Tables S6 and S7). We next performed a motif occurrence analysis of the 2507 co-occuring binding sites located in the 3′UTR of these 1370 genes (using FIMO (33) to identify the presence of our motif within these overlapping sites. Our analysis revealed the presence of our consensus motif (Figure 3B) in 858 sites within 602 genes (Supplementary Table S8). Our results, therefore, show that the YB1/HuR consensus motif is present in the 3′UTR of ∼36% and ∼44% of common mRNA targets in C2C12 and uroepithelial cells respectively (Figure 3F). These results thus suggest that the HuR/YB1 complex likely regulates the expression of common mRNAs by interacting with this consensus motif and that its regulatory role extends beyond the myogenic process.

We next performed Gene Ontology (GO) analysis on the 147 common RNAs containing the consensus site in muscle cells to determine the biological and functional importance of these shared messages. Classification of these transcripts by biological processes revealed that 3 of them, *Myog*, *MyoD* and c-*Myc*, encoded for proteins that were previously shown to be involved in skeletal muscle cell differentiation (9,81,82) (Supplementary Figure S3C, Table S9). Interestingly, all three of these mRNAs were previously shown to be posttranscriptionally regulated by HuR (20,22,83). We confirmed the presence of our consensus motif for YB1 and HuR binding in the 3′UTR of the mouse *Myog, MyoD* and *c-Myc* mRNA by sequence analysis (Figure 3G). Importantly we also confirmed the presence of this motif in the 3′UTR of the overlapping HuR and YB1 binding site in the human *c-Myc* gene (Supplementary Figure S3D,E).

To validate the association of *Myog, MyoD* and *c-Myc* mRNAs to YB1 and HuR in muscle cells we performed RNA-IP experiments coupled with RT-qPCR using antibodies against HuR or YB1 (Figure 3H). Our results show that both HuR and YB1 interact with these three mRNAs in muscle cells. Moreover we assessed binding of YB1 to these transcripts in the absence of HuR and, vice versa, the binding of HuR in YB1 depleted cells in order to investigate if HuR and YB1 depend on each other for their binding to these mRNAs. The knockdown of HuR significantly decreased, by >50%, YB1's association to the *Myog, MyoD* and *c-Myc* mRNAs (Figure 3I). Similarly, HuR's association to these transcripts was significantly reduced, by >50%, as a result of the depletion of endogenous YB1 (Figure 3J). These observations (coupled with the fact that YB1 and HuR interact in a RNA independent manner (Figure 1E), suggest that YB1 and HuR bind to each other prior

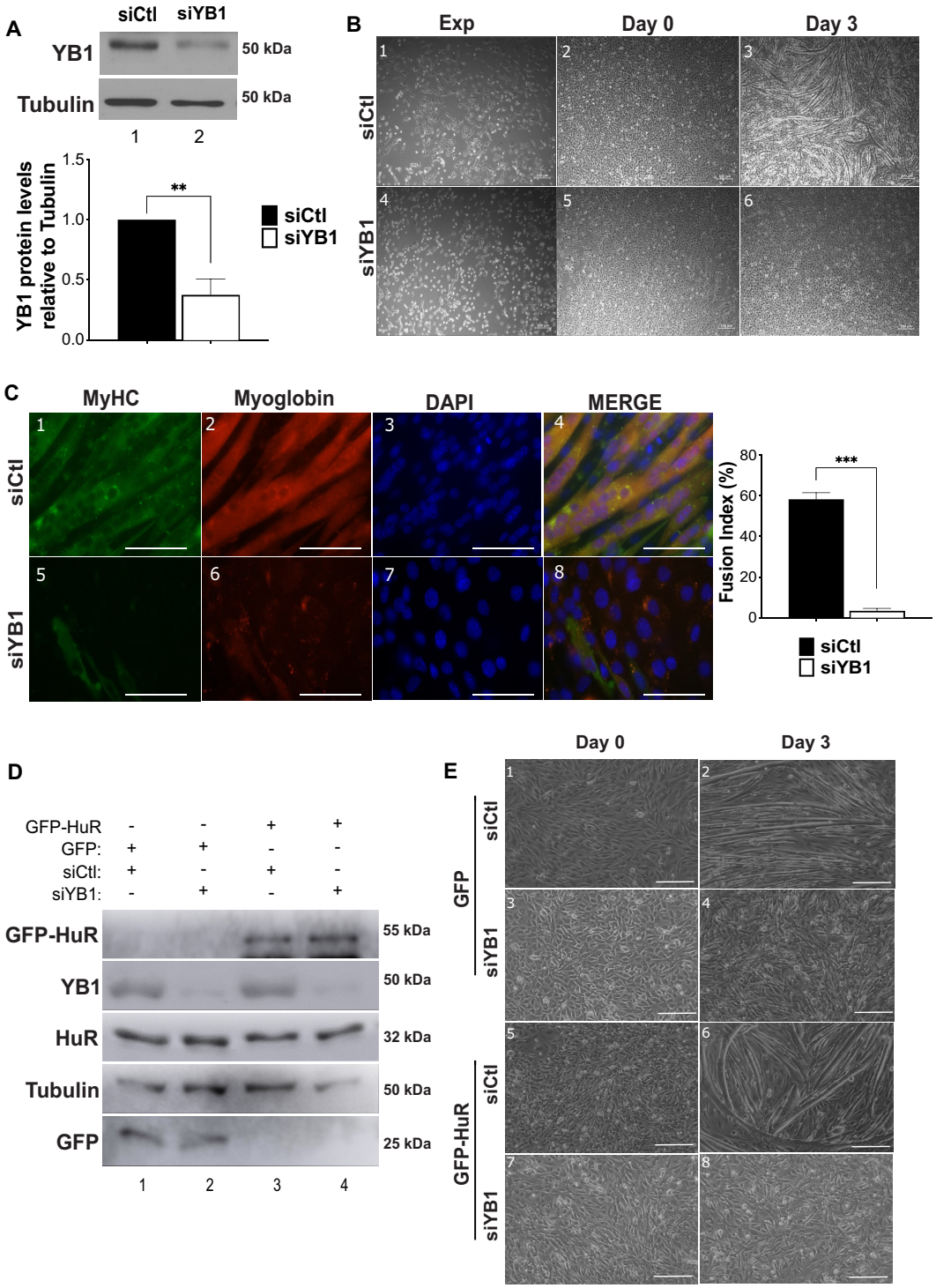

Figure 2. Depletion of YB1 prevents muscle cell differentiation. (**A**) C2C12 myoblasts were transfected with a siRNA targeting YB1 or a control siRNA. Top: western blot demonstrating the efficiency of YB1 knockdown. Blots were probed with antibodies against YB1 and α-tubulin (loading control). Bottom: quantification of YB1 protein levels relative to Tubulin. The band intensities were determined using ImageJ Software. Data are presented ± the SEM of three independent experiments. $^{**}P < 0.005$ (*t* test). (B, C) Effect of the depletion of YB1 in muscle cells on their differentiation capacity is shown. (**B**) Phase contrast pictures showing the differentiation status of C2C12 myoblasts (Exp as well as 0- and 3-day post-induction of differentiation) transfected with the siCtl or siYB1. Bars 50 μm. Images of a single representative field are shown. (**C**) Left: immunofluorescence images showing the differentiation status of siCtl and siYB1 treated cells at day 3 post-induction of the myogenic process using anti-MyHC and anti-Myoglobin antibodies and stained with DAPI. Images of a single representative field are shown. Bars 100 μm. Right: fusion index indicating the efficiency of C2C12 differentiation. Data are presented ± the SEM of three independent experiments. $^{***}P < 0.0005$ (*t* test). (D, E) C2C12 cells expressing GFP or GFP-HuR were depleted (siYB1) or not (siCtl) of YB1 and induced for differentiation for 3 days. (**D**) Cell extracts from these cells were used for western blot analysis with antibodies against HuR, YB1, GFP or α-tubulin (loading control). (**E**) Phase contrast pictures showing the differentiation status of these cells 0- and 3-day post-induction of differentiation. Bars 100 μm. Images of a single representative field are shown.

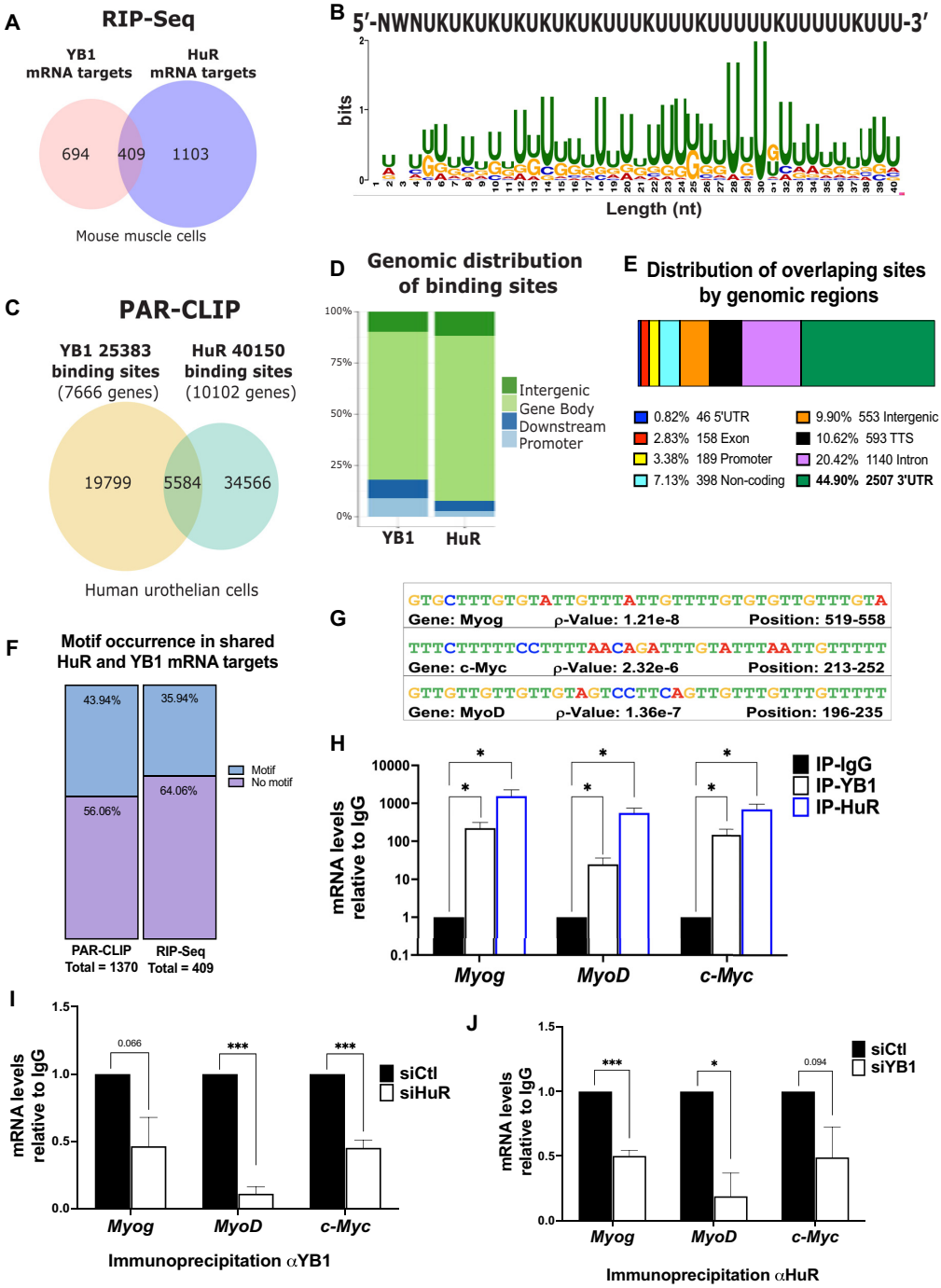

Figure 3. YB1 and HuR bind to common mRNA targets in muscle cells through a conserved motif. YB1 and HuR mRNA targets in C2C12 cells were identified by performing RIP-seq experiment ($N = 1$) using anti-HuR and anti-YB1 antibodies. (**A**) Venn diagram of common HuR and YB1 mRNA targets identified by RIP-seq. (**B**) Top: Fasta-formatted sequence of the 40nt consensus motif present in the 3′UTR of common YB1 and HuR mRNA targets in mice. Bottom: sequence logo of the 40bp consensus motif. The height of each letter represents the frequency of the base at corresponding position. (**C**) Venn diagram of shared binding sites for HuR and YB1 identified by analysis of pre-existing PAR-CLIP dataset. (**D**) Genome-wide distribution of HuR and YB1 binding sites as determined from PAR-CLIP dataset, the percentage of sites in each genomic class is indicated. (**E**) Genomic distribution of overlapping HuR and YB1 binding sites in the PAR-CLIP dataset. The percentage of sites in each genomic class is indicated. (**F**) Motif occurrence in mRNAs putatively co-regulated by YB1 and HuR, identified by RNA-seq or PAR-CLIP. (**G**) Truncated fasta-formatted sequence of the conserved motif identified in the 3′UTR of *Myog, c-Myc* and *MyoD* mRNAs. (**H**) Validation of binding of YB1 and HuR to common pro-myogenic mRNA targets. RNA was isolated from the IP of YB1 or HuR (IgG was used as a negative control) and RT-qPCR was performed using primers specific for *Myog*, *MyoD* and *cMyc* mRNAs. The normalized mRNA levels were then plotted relatively to the IP-IgG condition ± SEM of three independent experiments. $*P < 0.05$ (*t-test*). (I, J) IP experiments were performed on C2C12 cell lysates from siCtl, siHuR (**I**) or siYB1 (**J**) treated myoblast, using YB1 or HuR antibodies as well as IgG as control. RT-qPCR analysis were then performed using specific primers for *Myog, MyoD and c-Myc* mRNAs. For each IP sample, relative mRNA levels were standardized to the corresponding IP-IgG, normalized to the total mRNA levels in the input and then plotted relatively to siCtl condition. Data in 3H-J are presented ± the SEM of three independent experiments. $*P < 0.05$; $**P < 0.005$; $***P < 0.0005$ (*t*-test).

to their recruitment to the consensus motif in these target mRNAs.

YB1 and HuR stabilize *Myog, MyoD,* and *c-Myc* mRNAs via a U-rich consensus motif

We next investigated the mechanisms through which YB1 and HuR regulate these mRNAs. As a first step we assessed the effect of YB1 or HuR depletion on the steady state levels of the *Myog, MyoD* and *c-Myc* mRNAs. Similarly, to HuR, the depletion of YB1 significantly reduced, by >2-fold, *Myog, MyoD* and *c-Myc* mRNA levels in myotubes (Figure 4A). Next, we performed pulse-chase experiments using the RNA polymerase II inhibitor actinomycin D (ActD) to determine if the decrease in the steady state level of these messages was due to a decrease in their stability. We showed that the depletion of YB1, similarly to HuR, significantly decreased the stability of these mRNAs (Figure 4B–D). These results indicate that HuR and YB1 regulate the stability of common mRNA targets in muscle cells.

Sequence analysis of the *Myog* mRNA showed that the 3′UTR contains three G/U-rich elements (G/UREs 1, 2 and 3) (Figure 5A). We have previously shown that HuR associates, *in vitro,* to G/URE2 in the *Myog* mRNA 3′UTR (20). Interestingly, the consensus motif identified above in the *Myog* mRNA (Figure 3G) is located within this G/URE 2 region (Supplementary Figure S4A). To further dissect the molecular mechanism behind this YB1/HuR coregulatory function, as proof of principle, we decided to determine the role of the U-rich consensus sequence identified above in the stabilization of the *Myog* mRNA. As a first step, we determined if YB1, similarly to HuR, associates to the G/URE2 region (containing the consensus motif). We therefore performed RNA electromobility shift assays (REMSAs) using recombinant GST, GST-HuR or GST-YB1 proteins and radiolabeled RNA probes corresponding to the G/URE2 region as well as the other 2 putative G/UREs (Figure 5B). We observed that while GST-HuR forms a complex with the three elements, GST-YB1 predominately associated to G/URE2 (Figure 5B). The interaction of HuR to this probe appeares to be stronger than YB1. Consistent with our REMSA results, surface plasmon resonance (SPR) experiments performed using cDNA probes corresponding to the G/U-RE2 site and recombinant GST-HuR or GST-YB1 confirmed the association of HuR and YB1 with the G/URE2 site and showed that the binding affinity of HuR to this region was stronger than that of YB1 (as shown by a reduced equilibrium dissociation constant (KD)) (Supplementary Figure S4B). Together these results show that both HuR and YB1 directly associate, *in vitro*, to the same region within the *Myog* mRNA 3′UTR containing the consensus motif.

The importance of the U-rich consensus motif (Figure 3B,G) on the HuR/YB1 mediated regulation of *Myog* expression was further assessed using Renilla luciferase (Rluc) reporter constructs expressing either wild-type (pRL-*Myog*-3′UTR) or a mutant *Myog* mRNA 3′UTR in which G/URE2 (pRL-*Myog*-3′UTR-mut2) was deleted (Figure 5C, Supplementary Figure S4A). C2C12 cells were transfected with these Rluc-reporters as well as reporter constructs containing a deleted G/URE1 (pRL-*Myog*-3′UTR-mut1) or G/URE3 (pRL-*Myog*-3′UTR-mut3) region (used as negative controls) and the steady-state levels of the *Rluc* mRNAs were determined by RT-qPCR analysis. We observed that the levels of the pRL-*Myog*-3′UTR-mut2 mRNA, but not the pRL-*Myog*-3′UTR-mut1 or pRL-*Myog*-3′UTR-mut3 mRNAs, were 2-fold less than those observed with the wild-type pRL-*Myog*-3′UTR (Figure 5D). Luciferase activity assay (which is proportional to Rluc protein levels) showed that, similarly to the mRNA levels, the luciferase activity of the pRL-*Myog*-3′UTR-mut2 reporter (but not the other 2 mutants) was significantly lower than the wild-type pRL-*Myog*-3′UTR counterpart (Figure 5E). Additionally, the half-life of the pRL-*Myog*-3′UTR-mut2 mRNA, but not the other two mutants, was significantly reduced when compared to the wild-type pRL-*Myog*-3′UTR mRNA (Figure 5F). Finally, RNA-IP coupled to RT-qPCR experiments demonstrated that the association of YB1 and HuR to the pRL-*Myog*-3′UTR-mut2 mRNA, but not the other constructs, was significantly decreased by >2-fold due to the deletion of the G/URE2 element (Figure 5G, H).

We next assessed the importance of YB1/HuR binding to the G/URE2 element on the regulation of the full-length *Myog* transcript. We generated GFP-conjugated Myog plasmids expressing full-length (GFP-Myog) or mutated variants of the Myog protein in which G/URE1, 2 or 3 were deleted (GFP-Myog-mut1, GFP-Myog-mut2, GFP-Myog-mut3) (Figure 6A). These Myog variants were expressed in C2C12 cells and GFP-Myog protein levels were assessed by IF and WB (Figure 6B, C). As expected, deletion of G/URE1 or G/URE3 did not affect GFP-Myog expression. By contrast, deletion of the G/URE2 element decreased, by >2-fold, GFP-Myog protein levels (Figure 6C). Interestingly, the effect of mutating the G/URE2 on the expression of exogenous GFP-Myog was similar to the effect of knocking down HuR (20) or YB1 on endogenous Myog protein levels (Figure 6D). Taken together our results indicate that the HuR/YB1 complex regulates the stability of the *Myog* mRNA by associating with a U-rich consensus site in the 3′UTR.

The interaction between HuR and YB1 is required for the regulation of *Myog* expression

To further delineate the mechanism of YB1/HuR-mediated mRNA stabilization of *Myog* mRNA we set out to determine the region of HuR required for its binding to YB1. By performing computational modeling assessing the formation of a ternary molecular complex we identified a potential YB1 binding motif (spanning amino acids 227–234) in HuR (Supplemental Figure S5A,B, Figure 7A top). In order to validate the importance of this motif we generated plasmids expressing GFP-tagged wild-type HuR (GFP-HuR) or a HuR mutant deleted of the amino acids 227–234 (GFP-HuR-M1) that may constitute a YB1 binding site (Figure 7A bottom). IP experiments with the anti-YB1 antibody using C2C12 extracts transfected with these plasmids showed that, contrary to GFP-HuR, GFP-HuR-M1 was unable to associate to YB1 (Figure 7B). In addition, IP/RT-qPCR experiments showed that while GFP-HuR strongly associated to the *Myog* mRNA, GPF-HuR-M1 failed to bind with the

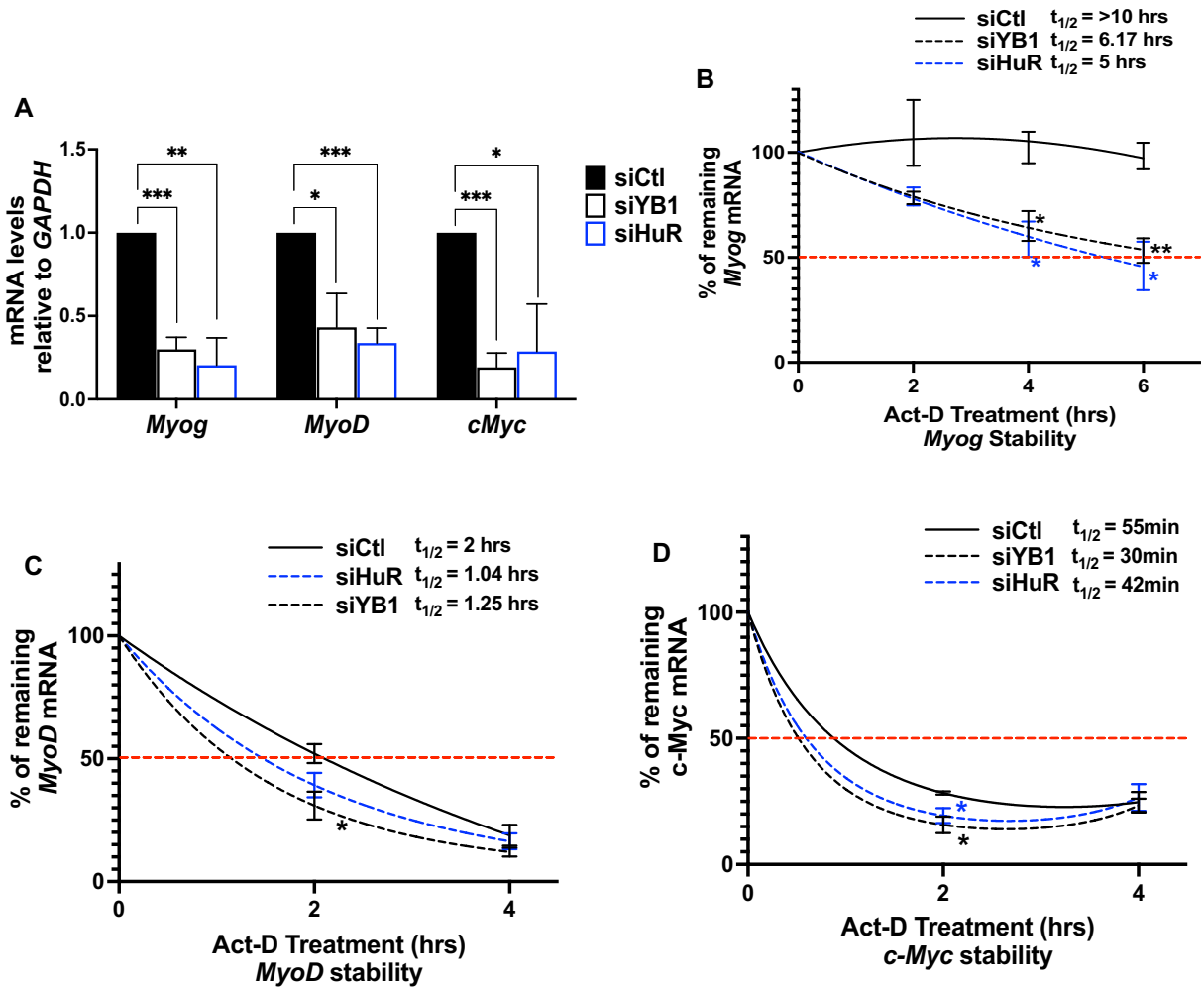

Figure 4. YB1 and HuR regulates the stability of common mRNA targets containing a U-rich consensus site. (**A**) Exponentially growing C2C12 cells treated with siRNAs targeting YB1 (siYB1), HuR (siHuR) or treated with a control siRNA (siCtl) were used to assess *Myog*, *MyoD,* and *cMyc* mRNAs steady-state levels. mRNA levels were assessed by RT-qPCR using specific primers, standardized against *GAPDH* mRNA levels and plotted relative to the siCtl condition. Data are presented ± the SEM of three independent experiments. *$P < 0.05$, **$P < 0.005$, ***$P < 0.0005$ (*t*-test) (**B–D**) The stability of the *Myog*, *MyoD* and *cMyc* mRNAs in C2C12 cells depleted or not (siCtl) of YB1 (siYB1) or HuR (siHuR) was determined by ActD pulse-chase experiments. Cells were treated with Actinomycin D (ActD) for 0, 2, 4 or 6 h and total RNA was used for RT-qPCR analysis. The expression level of the mRNA in each time point was normalized to *GAPDH* mRNA levels and plotted relative to the abundance of each message at 0 h of ActD treatment (considered to be 100%). Data in the figure are presented ± the SEM of three independent experiments. *$P < 0.05$, **$P < 0.005$ (*t*-test)

transcript (Figure 7C). Overexpressing the GFP-HuR but not the GFP-HuR-M1 isoform significantly increased the expression of *Myog* mRNA (Figure 7D). Moreover, our IF experiments showed that the GFP-HuR-M1 variant, unlike GFP-HuR, was unable the rescue the differentiation of C2C12 myoblasts depleted of HuR (Figure 7E). Taken together our data indicate that the formation of a HuR/YB1 complex regulates the expression of pro-myogenic mRNAs such as *Myog* during the pre-terminal stage of myogenesis by binding to a U-rich consensus motif in the 3′UTR.

DISCUSSION

HuR-mediated regulation of myogenesis was one of the first examples of a role of a posttranscriptional regulator in muscle fiber formation (13,31). Previous work have established that HuR does so by posttranscriptionally regulating the expression of several classic (MyoD, Myog and p21) (20,22) and newly identified modulators of myogenesis (HMGB1, NPM) (26,27). First described as a positive regulator of mRNA stability, we now know that HuR can have multiple and sometime opposite functions on it targeted transcripts, switching from a promoter of translation (24,26) to a mRNA stabilizer (20–22,33,35) or to a promoter of mRNA decay (25,27). Numerous reports have indicated that the versatility of HuR function is dictated by its collaboration or competition with other trans-acting factors (13,23–26,27) While the mechanisms by which HuR and other RBPs regulate mRNA translation and decay is well studied, the way by which HuR stabilizes its target mRNA remains elusive. Thus, identifying the network of trans-acting factors that interact with HuR and the mechanisms through which they regulate mRNA stability is paramount

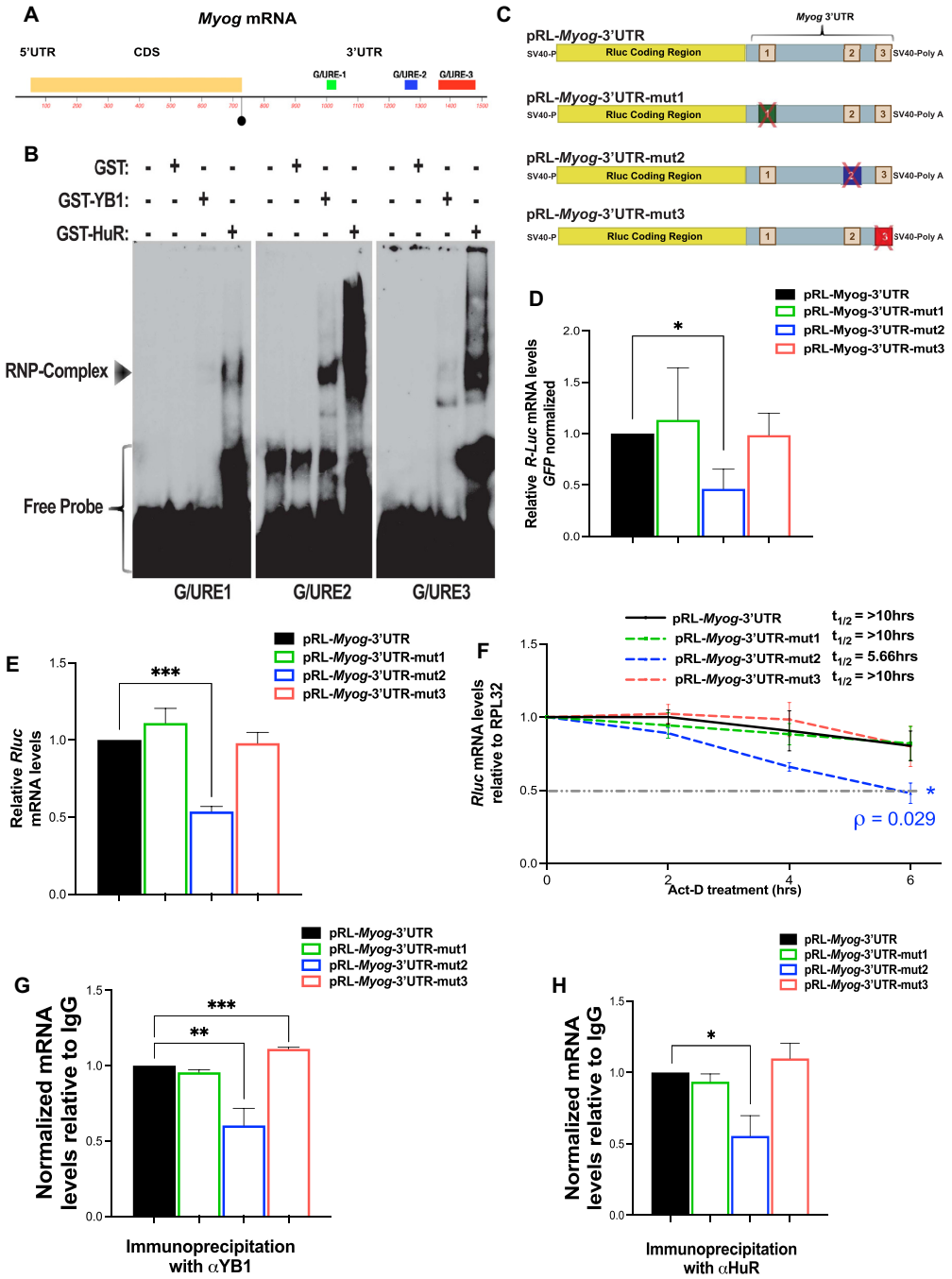

Figure 5. YB1 and HuR binding to a consensus motif in the 3′UTR of the *Myog* mRNA is required for its stabilization. (**A**) Schematic representation of the *Myog* mRNA sequence. *Myog* coding sequence is highlighted in yellow (Nucleotide 53–727). The first nucleotide of the 3′UTR (nucleotide 728) is marked with a black circle. G/U-Rich Elements (G/URE) present in the *Myog* 3′UTR are shown as colored boxed; G/URE1 is highlighted in green (nucleotide 1001–1030), G/URE2 (containing the consensus motif described in Figure 3B) is highlighted in blue (nucleotide 1251–1290), and G/URE 3 is highlighted in red (nucleotide 1359–1479). (**B**) RNA electromobility shift assays (REMSA) were performed with radiolabeled G/URE 1, 2 and 3 cRNA probes which were incubated with purified GST, GST-YB1 or GST-HuR protein. (**C**) Schematic representation of the Rluc reporter constructs containing the *Myog* mRNA 3′UTR with or without deletion of the G/URE 1, 2 or 3 regions (indicated by colored blocks). (**D**) Exponentially growing C2C12 cells were transfected with the reporter constructs described in (C). Total RNA was isolated from these cells 2 days after induction of differentiation and the expression levels of Rluc mRNA was determined by RT-qPCR. Expression levels of the mutant Rluc reporters was standardized against *RPL32* mRNA levels and plotted relative to the expression of the wild type pRL-*Myog*-3′UTR reporter. (**E**) Total cell extracts from C2C12 cells expressing the Rluc reporters described above were used to determine Luciferase activity. (**F**) The stability of the Rluc RNA reporters was determined by ActD pulse-chase experiments. Cells were treated with Actinomycin D (ActD) for 0, 2, 4 or 6 h and total RNA used for RT-qPCR analysis. The expression level of the *Rluc* mRNA in each time point was determined relative to *RPL32* mRNA levels and plotted relative to the abundance of each message at 0 hrs. of ActD treatment, which is considered as 100% (G–H) Lysates from cells expressing the Rluc reporters were used for RIP-coupled to RT-qPCR experiments using the anti-YB1 or anti-HuR antibody. The amount of *Rluc* mRNA associated to (**G**) YB1 or (**H**) HuR was determined by RT-qPCR and normalized to total *Rluc* mRNA in the input. Data in (D)–(H) is presented ± the SEM of three independent experiments. $^{*}P < 0.05$; $^{**}P < 0.005$; $^{***}P < 0.0005$ (*t*-test).

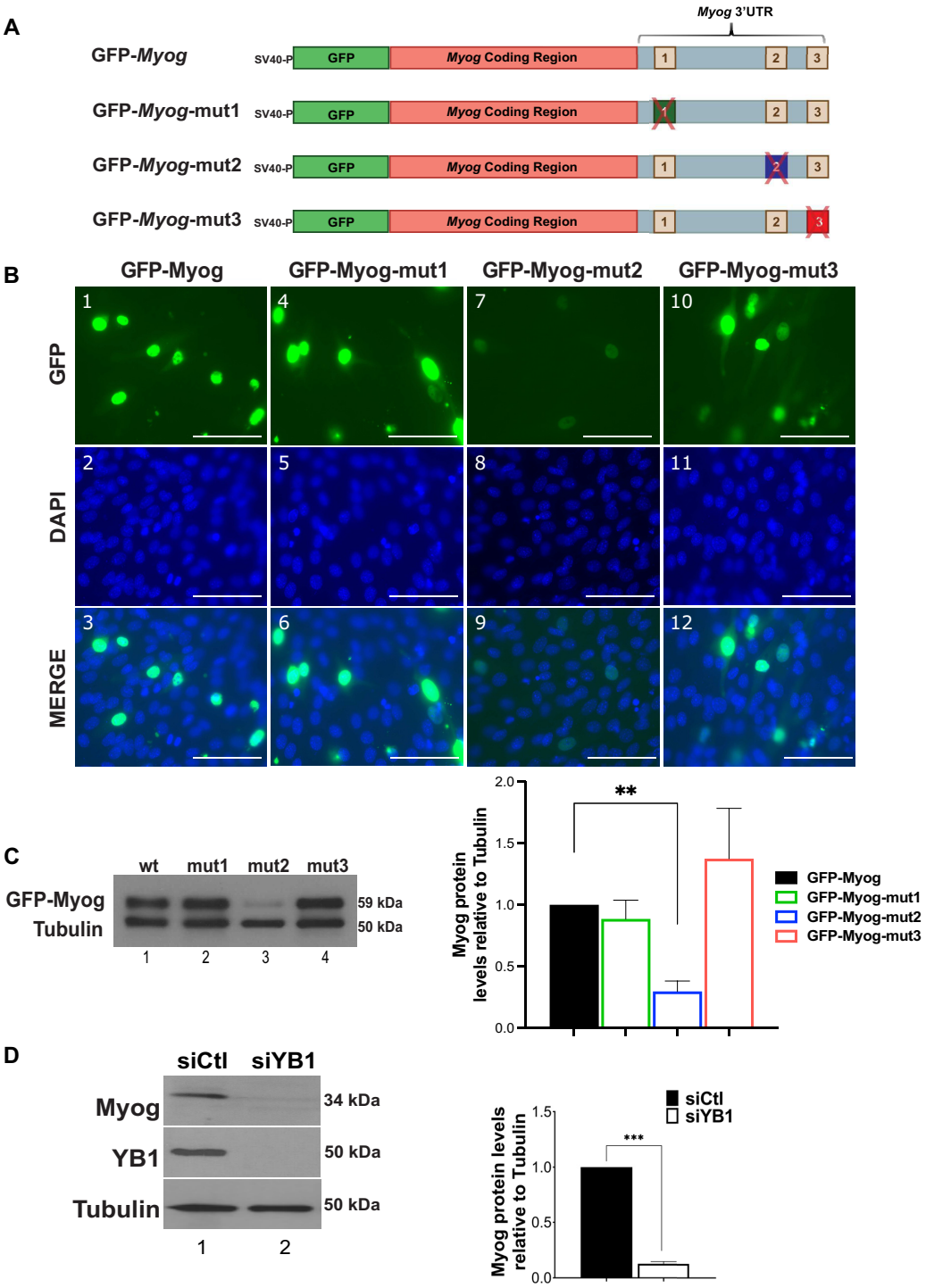

Figure 6. The consensus motif mediating binding of theYB1/HuR complex is required for the regulation of Myog expression. (**A**) Schematic representation of the GFP constructs containing the full length *Myog* cDNA with or without deletion of the G/URE 1, 2 or 3 (indicated by colored blocks). (**B**) Exponentially growing C2C12 cells transfected with the reporter constructs described above were visualized by IF after DAPI staining. (**C**) Exponentially growing C2C12 cells were transfected with the reporter constructs described above. Left: lysates from these cells were then analyzed by western blot using antibodies against GFP and α-tubulin (loading control) to assess GFP-Myog protein levels. Right: quantification of GFP-Myog protein levels normalized to Tubulin are shown relative to wild-type GFP-Myog containing the 3′UTR. The band intensities were determined using ImageJ Software. (**D**) Exponentially growing C2C12 cells depleted (siYB1) or not (siCtl) of YB1 were used to assess Myog protein levels. Left: WB demonstrating the efficiency of YB1 knockdown and Myog protein levels in C2C12 extracts collected at day 2 post-induction of the differentiation process. Blots were probed with antibodies against Myog, YB1 and α-tubulin (loading control). Right: quantification of Myog protein levels relative to Tubulin. The band intensities were determined using ImageJ Software. Data in (B) and (D) are presented ± the SEM of three independent experiments. $^{**}P < 0.005$; $^{***}P < 0.0005$ (*t*-test).

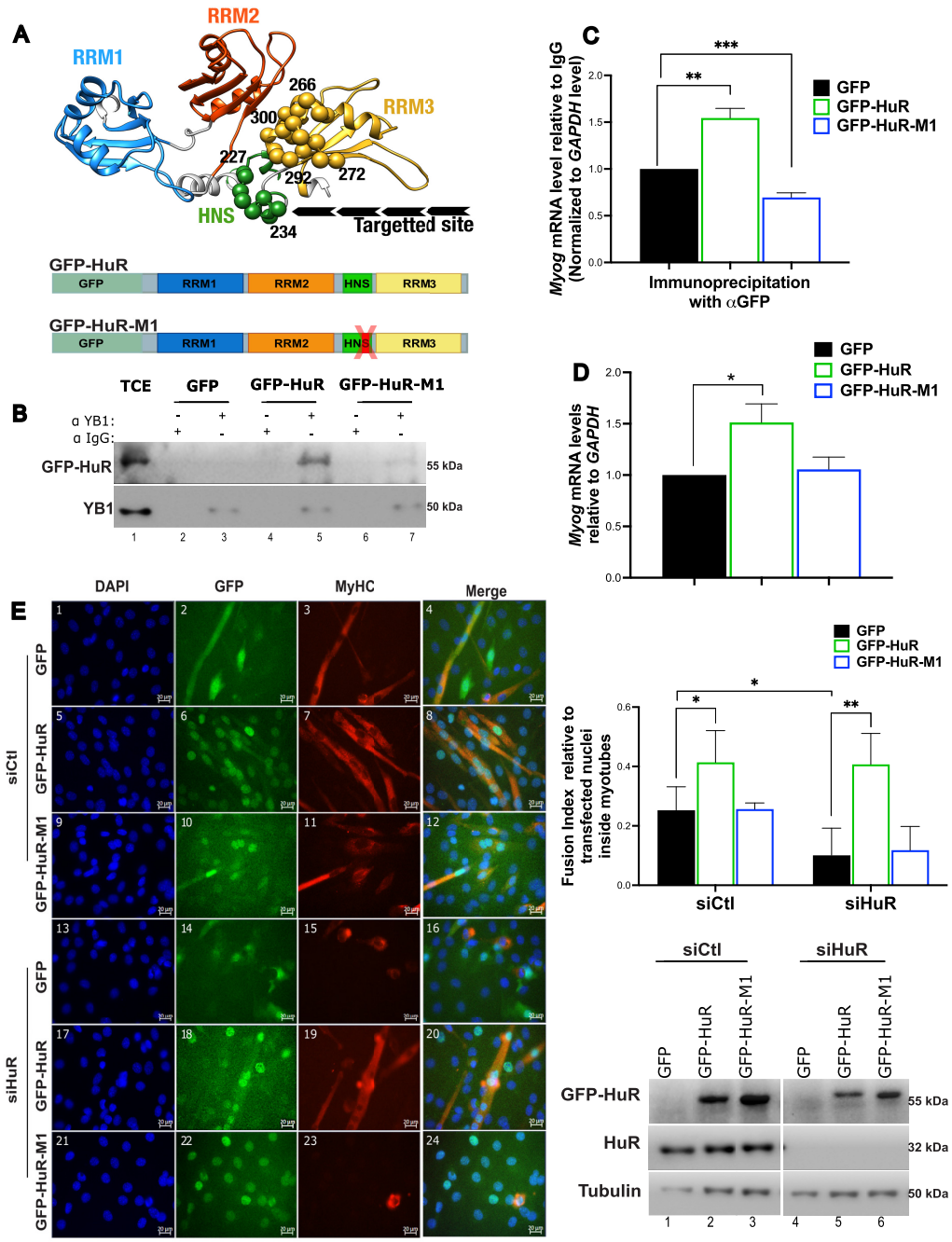

Figure 7. The interaction of HuR and YB1 is required for the HuR-mediated expression of mRNA targets. (**A**) top; Illustration of the HuR protein residues that form the interface with YB1. The RRM domains of HuR are encoded in blue, orange and yellow respectively, as well as HNS in green. The protein residues that form the interface with YB1 are shown as spheres and are numbered accordingly with its protein sequence number. Bottom: schematic representation of the GFP constructs expressing the GFP-tagged WT HuR (GFP-HuR) or the GFP-HuR mutant variant in which the computational determined amino acids (227–234) that interact with YB1 have been deleted (GFP-HuR-M1). HuR protein domains are indicated by colored blocks consistent with top panel. (B, C) IP experiments (using the YB1 antibody or IgG as a control) on total cell extracts collected 24 h post-induction of differentiation of C2C12 muscle cells transfected with GFP, GFP-HuR or GFP-HuR-M1 plasmids. (**B**) The input (TCE) and the immunoprecipitates were analyzed by western blot using antibodies against HuR, and YB1. (**C**) RIP-coupled to RT-qPCR experiments using an anti-GFP antibody and cells transfected as described above were performed to assess the levels of *Myog* mRNA associated to GFP-HuR or GFP-HuR-M1. Levels were standardized against *GAPDH* mRNA and plotted relative to the GFP control condition ± SEM of three independent experiments. (**D**) Total RNA was isolated from cells transfected with GFP, GFP-HuR or GFP-HuR-M1 plasmids 2 days post-induction of differentiation. The *Myog* mRNA levels in these cells was determined by RT-qPCR. Expression levels of the *Myog* mRNA was standardized against *GAPDH* mRNA levels and plotted relative to the expression seen in GFP transfected cells. (**E**) Immunofluorescence images (stained with anti-MyHC and anti-GFP antibodies, as well as with DAPI to stain nuclei) of cells treated with siCtl or siHuR and expressing GFP, GFP-HuR or GFP-HuR-M1. Images of a single representative field are shown. Bars 100 μm. Right-top: fusion index indicating the efficiency of C2C12 differentiation. Right-bottom: western blot demonstrating the efficiency of HuR silencing and expression of GFP-HuR or GFP-HuR-M1 in siCtl and siHuR treated C2C12 myoblast. Blots were probed with antibodies against HuR, GFP and α-tubulin (loading control). Data in (D) and (E) are presented ± the SEM of three independent experiments. *$P < 0.05$; **$P < 0.005$; ***$P < 0.0005$ (*t*-test).

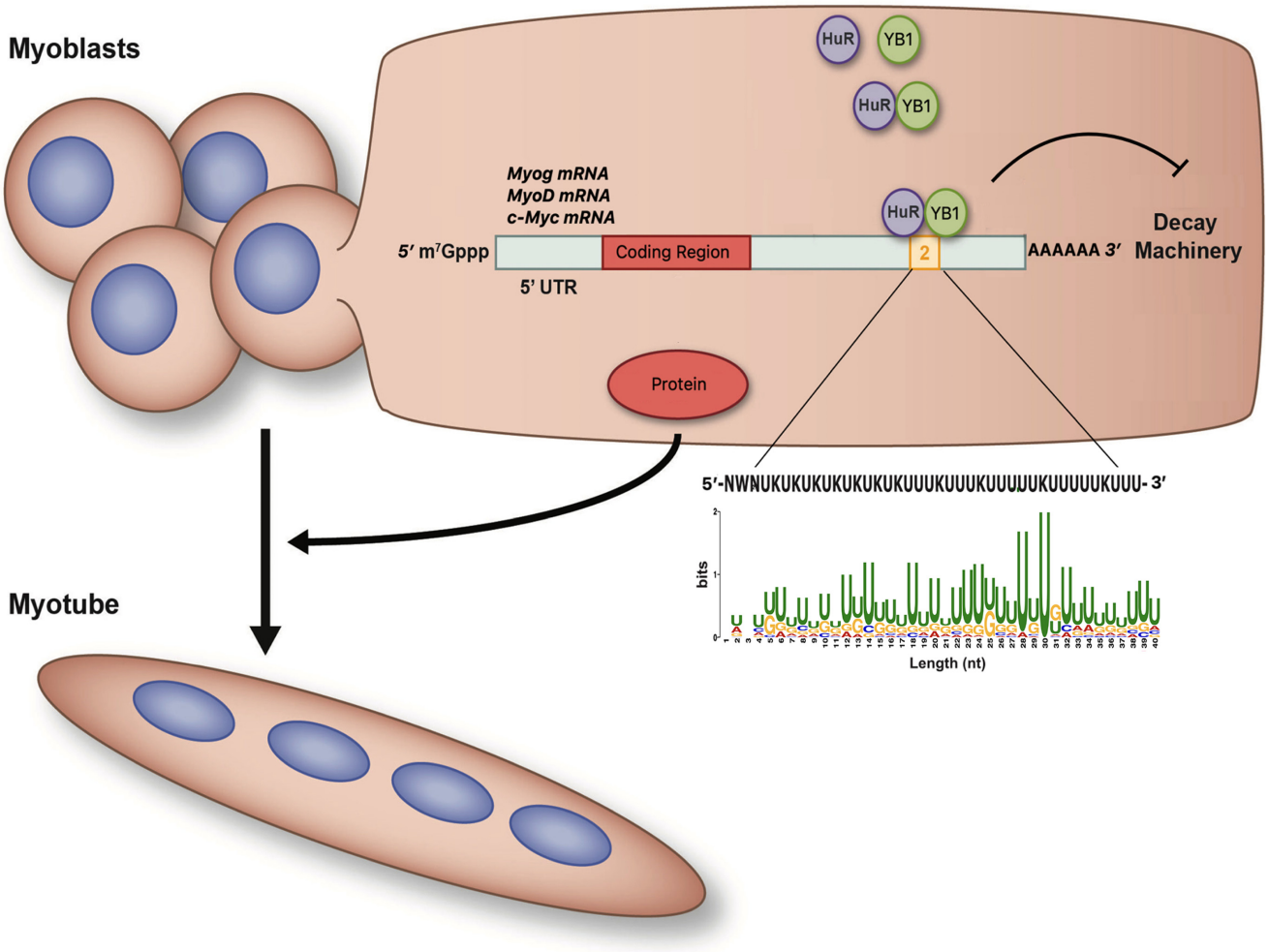

Figure 8. Model depicting the molecular mechanism through which the HuR and YB1 complex regulates mRNA stability to promote muscle fiber formation. During the transition step from myoblast to myotubes, HuR associates to the YB1 protein in an RNA independent manner. This complex is then recruited to a consensus motif in the 3′ UTR of target mRNAs such as *Myog*, *MyoD* and *c-Myc*. In doing so, the HuR/YB1 complex increases the stability of these *mRNAs* resulting in the concomitant formation and maintenance of muscle fibers.

to our understanding of HuR function in physiological processes such as myogenesis.

Herein, mass spectrometry (MS)-based approaches have enabled us to uncover a network of HuR-protein partners during the pre-terminal stage of the myogenic process, highlighting YB1 as a central player in mediating the function of HuR during myogenesis. Our analysis showed that HuR had the greatest affinity for proteins with RNA/DNA binding activity (Figure 1B, C). The fact that some of these identified ligands localized within ribonucleoprotein complexes (Supplementary Figure S1A) provides further evidence that many physiological processes, such as myogenesis, may be regulated by an interplay between RBPs rather than by the individualities of single regulators. Additionally, next generation sequencing-based methodologies enabled the transcriptome-wide identification of mRNA targets co-regulated by HuR and YB1. The observation that approximately one-third of these target transcripts, contain a newly identified U-rich consensus motif within their 3′UTR (Figure 3B,F) suggests that the effect of the HuR/YB1 complex in muscle fiber formation is the result of the concerted regulation of a common set of genes containing this consensus site. Furthermore, the conservation of the U-rich consensus binding motif across different cell types and species (Figure 3C–F, Supplementary Figure S3B-E), indicates that this motif may serve as a general physiological signal to promote mRNA stabilization via the recruitment of the HuR/YB1 stabilizing complex. Together our data support a model whereby, during the transition step from myoblast to myotubes, HuR interacts with YB1 in an RNA independent manner. This complex is then recruited to a defined, conserved regulatory element located in the 3′UTR of target mRNAs leading to their stabilization, thus resulting in the concomitant formation and maintenance of muscle fibers (Figure 8). In doing so our study further supports the growing evidence that the functional diversity of HuR-mediated regulation relies in its ability to associate with different trans-acting partners (19,24–27) allowing a fine tuning of the posttranscriptional program during myogenesis.

Recently, Chen *et al.* demonstrated that YB1 mediates the stability of mRNAs containing 5-methylcytosine residues in uroepithelial cells (46). These modified residues were predominately located in the coding region, typically downstream of translation initiation sites in these mRNAs (46). They, furthermore, show that YB1 stabilizes these mRNAs (containing the modified cytosine residues) by recruiting HuR. However, this study did not assess whether the stability of these modified mRNA requires the RNA-independent interaction of both HuR and YB1. Our data, on the other hand, clearly establish that the formation of a YB1/HuR complex is required for the stability of common target messages during a physiological process such as muscle fiber formation. Interestingly, by analysing PAR-CLIP dataset reported in this study, we observed that the U-rich consensus site we identified in our study is present in the 3′UTR of ∼44% of common HuR/YB1 mRNA targets in these cells (Figure 3F). This result is similar to what was observed in our muscle cells whereby the consensus site was found in the 3′UTR of 36% of common mRNA targets. The data presented from the manuscript published by Chen et.al. and our present study therefore suggests that YB1/HuR may regulate the stability of distinct mRNAs subsets through different mechanisms that are dictated by the nature of the *cis*-element (modified methylcytosine residues versus the consensus binding site) these RBPs interact with. The selective mechanism through which the YB1/HuR complex regulates these two distinct mRNA subsets, however, is likely dependent on the way by which HuR and YB1 interact. While the reason behind the existence of two YB1/HuR stabilizing mechanisms remains unclear, it is evident that both play an important role in stabilizing distinct subsets of mRNAs.

Our work provides the first demonstration that YB1 is implicated in the HuR-mediated regulation of muscle fiber formation. What remains unknown, however, at this point, is if this HuR-mediated stabilizing complex involves, in addition to YB1, the recruitment of other RBPs that were shown in this study (Figure 1C, D) to bind to HuR. Our observations, thus, suggest that the complexity of mechanisms mediating the stability of mRNAs may rival that of transcriptional regulation or mRNA decay pathways in several, if not all, physiological processes.

DATA AVAILABILITY

The data reported in this study in support of all the findings outlined are available from the corresponding author upon reasonable request. Raw sequences from RNA-Seq experiments are deposited on the Gene Expression Omnibus (GEO) database repository from The National Center for Biotechnology Information (NCBI) under the accession number GSE178419.

SUPPLEMENTARY DATA

Supplementary Data are available at NAR Online.

ACKNOWLEDGEMENTS

We would like to thank Derek Hall and Amr Omer for their help in reviewing and editing the manuscript.

Author contributions: B.J.S. contributed to the design and implementation of the research, carried out data acquisition and/or analysis of all the experiments, wrote the original draft of the manuscript. S.M. assisted with sample preparation as well as acquisition of most of the experimental data. S.B. carried out the motif discovery analysis and assisted in data acquisition for Figure 3. Y.L.S designed and performed the modeling of the protein-protein-RNA complex and assisted in data acquisition for Figure 7. X.J.L. provided technical expertise and help in sample preparation and data acquisition for Figures 5 and 6. K.A assisted in sample preparation and data acquisition. J.S. performed RIP-MS experiment and assisted in its analysis. S.D. and S.K. contributed with the conceptualization, data analysis, and helped edit and review the manuscript. I.-E.G. designed, directed and supervised the study.

FUNDING

CIHR operating grant [MOP-142399]; CIHR project grant [PJT-159618 to I.E.G.]; B.J.S. was funded by a scholarship received from the Concejo Nacional de Ciencia y Tecnologia (CONACyT); Fonds de recherche du Québec—Nature et technologies (FRQNT); S.M. was funded by a Charlotte and Leo Karrasik Graduate Studentship; S.B.was funded by a scholarship received from the Natural Sciences and Engineering Research Council of Canada; K.A. was funded by a scholarship received from Taibah University-Ministry of Higher education. J.S. was supported by CIHR Studentship Award [GSD-164154]. Funding for open access charge: CIHR Project Grant [PJT-159618].
Conflict of interest statement. None declared.

REFERENCES

1. Tallquist,M.D., Weismann,K.E., Hellstrom,M. and Soriano,P. (2000) Early myotome specification regulates PDGFA expression and axial skeleton development. *Development*, **127**, 5059–5070.
2. Fan,C.M., Li,L., Rozo,M.E. and Lepper,C. (2012) Making Skeletal Muscle from Progenitor and Stem Cells: development versus Regeneration. *Wiley Interdiscip Rev Dev Biol*, **1**, 315–327.
3. Bentzinger,C.F., Wang,Y.X. and Rudnicki,M.A. (2012) Building muscle: molecular regulation of myogenesis. *Cold Spring Harb. Perspect. Biol.*, **4**, a008342.
4. Charge,S.B. and Rudnicki,M.A. (2004) Cellular and molecular regulation of muscle regeneration. *Physiol. Rev.*, **84**, 209–238.
5. Tapscott,S.J. and Weintraub,H. (1991) MyoD and the regulation of myogenesis by helix-loop-helix proteins. *J. Clin. Invest.*, **87**, 1133–1138.
6. Wang,Y. and Jaenisch,R. (1997) Myogenin can substitute for Myf5 in promoting myogenesis but less efficiently. *Development*, **124**, 2507–2513.
7. Bentzinger,C.F., Wang,Y.X., von Maltzahn,J. and Rudnicki,M.A. (2012) The emerging biology of muscle stem cells: implications for cell-based therapies. *Bioessays.*, **35**, 231–241.
8. Rudnicki,M.A., Le Grand,F., McKinnell,I. and Kuang,S. (2008) The molecular regulation of muscle stem cell function. *Cold Spring Harb. Symp. Quant. Biol.*, **73**, 323–331.
9. Asfour,H.A., Allouh,M.Z. and Said,R.S. (2018) Myogenic regulatory factors: the orchestrators of myogenesis after 30 years of discovery. *Exp. Biol. Med. (Maywood)*, **243**, 118–128.
10. Kaeser,M.D. and Emerson,B.M. (2006) Remodeling plans for cellular specialization: unique styles for every room. *Curr. Opin. Genet. Dev.*, **16**, 508–512.
11. Figliola,R., Busanello,A., Vaccarello,G. and Maione,R. (2008) Regulation of p57(KIP2) during muscle differentiation: role of Egr1, Sp1 and DNA hypomethylation. *J. Mol. Biol.*, **380**, 265–277.

12. Apponi,L.H., Corbett,A.H. and Pavlath,G.K. (2011) RNA-binding proteins and gene regulation in myogenesis. *Trends Pharmacol. Sci.*, **32**, 652–658.
13. Figueroa,A., Cuadrado,A., Fan,J., Atasoy,U., Muscat,G.E., Munoz-Canoves,P., Gorospe,M. and Munoz,A. (2003) Role of HuR in skeletal myogenesis through coordinate regulation of muscle differentiation genes. *Mol. Cell. Biol.*, **23**, 4991–5004.
14. Phillips,B.L., Banerjee,A., Sanchez,B.J., Di Marco,S., Gallouzi,I.E., Pavlath,G.K. and Corbett,A.H. (2018) Post-transcriptional regulation of Pabpn1 by the RNA binding protein HuR. *Nucleic Acids Res.*, **46**, 7643–7661.
15. von Roretz,C., Macri,A.M. and Gallouzi,I.E. (2011) Transportin 2 regulates apoptosis through the RNA-binding protein HuR. *J. Biol. Chem.*, **286**, 25983–25991.
16. Schaefke,B., Sun,W., Li,Y.S., Fang,L. and Chen,W. (2018) The evolution of posttranscriptional regulation. *Wiley Interdisciplinary Reviews. RNA*., **9**, e1485.
17. Ji,Y. and Tulin,A.V. (2013) Post-transcriptional regulation by poly(ADP-ribosyl)ation of the RNA-binding proteins. *Int. J. Mol. Sci.*, **14**, 16168–16183.
18. Abdelmohsen,K., Kuwano,Y., Kim,H.H. and Gorospe,M. (2008) Posttranscriptional gene regulation by RNA-binding proteins during oxidative stress: implications for cellular senescence. *Biol. Chem.*, **389**, 243–255.
19. Beauchamp,P., Nassif,C., Hillock,S., van der Giessen,K., von Roretz,C., Jasmin,B.J. and Gallouzi,I.E. (2010) The cleavage of HuR interferes with its transportin-2-mediated nuclear import and promotes muscle fiber formation. *Cell Death Differ.*, **17**,1588–1599.
20. van der Giessen,K., Di-Marco,S., Clair,E. and Gallouzi,I.E. (2003) RNAi-mediated HuR depletion leads to the inhibition of muscle cell differentiation. *J. Biol. Chem.*, **278**, 47119–47128.
21. Di Marco,S., Mazroui,R., Dallaire,P., Chittur,S., Tenenbaum,S.A., Radzioch,D., Marette,A. and Gallouzi,I.E. (2005) NF-kappa B-mediated MyoD decay during muscle wasting requires nitric oxide synthase mRNA stabilization, HuR protein, and nitric oxide release. *Mol. Cell. Biol.*, **25**, 6533–6545.
22. van der Giessen,K. and Gallouzi,I.E. (2007) Involvement of transportin 2-mediated HuR import in muscle cell differentiation. *Mol. Biol. Cell*, **18**, 2619–2629.
23. Cammas,A., Sanchez,B.J., Lian,X.J., Dormoy-Raclet,V., van der Giessen,K., Lopez de Silanes,I., Ma,J., Wilusz,C., Richardson,J., Gorospe,M. *et al.* (2014) Destabilization of nucleophosmin mRNA by the HuR/KSRP complex is required for muscle fibre formation. *Nat. Commun.*, **5**, 4190.
24. von Roretz,C., Beauchamp,P., Di Marco,S. and Gallouzi,I.E. (2011) HuR and myogenesis: being in the right place at the right time. *Biochim. Biophys. Acta*, **1813**, 1663–1667.
25. Janice Sanchez,B., Tremblay,A.K., Leduc-Gaudet,J.P., Hall,D.T., Kovacs,E., Ma,J.F., Mubaid,S., Hallauer,P.L., Phillips,B.L., Vest,K.E. *et al.* (2019) Depletion of HuR in murine skeletal muscle enhances exercise endurance and prevents cancer-induced muscle atrophy. *Nat. Commun.*, **10**, 4171.
26. Dormoy-Raclet,V., Cammas,A., Celona,B., Lian,X.J., van der Giessen,K., Zivojnovic,M., Brunelli,S., Riuzzi,F., Sorci,G., Wilhelm,B.T. *et al.* (2013) HuR and miR-1192 regulate myogenesis by modulating the translation of HMGB1 mRNA. *Nat. Commun.*, **4**, 2388.
27. Cammas,A., Sanchez,B.J., Lian,X.J., Dormoy-Raclet,V., van der Giessen,K., de Silanes,I.L., Ma,J., Wilusz,C., Richardson,J., Gorospe,M. *et al.* (2014) Destabilization of nucleophosmin mRNA by the HuR/KSRP complex is required for muscle fibre formation. *Nat. Commun.*, **5**, 4190.
28. Lejeune,F. (2022) Nonsense-Mediated mRNA Decay, a Finely Regulated Mechanism. *Biomedicines*, **10**, 141.
29. Adjibade,P. and Mazroui,R. (2014) Control of mRNA turnover: implication of cytoplasmic RNA granules. *Semin. Cell Dev. Biol.*, **34**, 15–23.
30. Scott,D.D., Aguilar,L.C., Kramar,M. and Oeffinger,M. (2019) It's Not the destination, it's the journey: heterogeneity in mRNA export mechanisms. *Adv. Exp. Med. Biol.*, **1203**, 33–81.
31. Hernández,G., García,A., Sonenberg,N. and Lasko,P. (2020) Unorthodox mechanisms to initiate translation open novel paths for gene expression. *J. Mol. Biol.*, **432**, 166702.
32. Liu,Q., Fang,L. and Wu,C. (2022) Alternative splicing and isoforms: from mechanisms to diseases. *Genes (Basel)*, **13**, 401.
33. Rothamel,K., Arcos,S., Kim,B., Reasoner,C., Lisy,S., Mukherjee,N. and Ascano,M. (2021) ELAVL1 primarily couples mRNA stability with the 3′ UTRs of interferon-stimulated genes. *Cell Rep.*, **35**, 109178.
34. Kang,S., Lee,T.A., Ra,E.A., Lee,E., Choi,H., Lee,S. and Park,B. (2014) Differential control of interleukin-6 mRNA levels by cellular distribution of YB-1. *PLoS One*, **9**, e112754.
35. Sundaram,G.M., Quah,S., Guang,L.G. and Sampath,P. (2021) HuR enhances FSTL1 transcript stability to promote invasion and metastasis of squamous cell carcinoma. *Am. J. Cancer Res.*, **11**, 4981–4993.
36. Kohno,K., Izumi,H., Uchiumi,T., Ashizuka,M. and Kuwano,M. (2003) The pleiotropic functions of the Y-box-binding protein, YB-1. *Bioessays*, **25**, 691–698.
37. Song,Y.J. and Lee,H. (2010) YB1/p32, a nuclear Y-box binding protein 1, is a novel regulator of myoblast differentiation that interacts with Msx1 homeoprotein. *Exp. Cell. Res.*, **316**, 517–529.
38. Zhang,Y.F., Homer,C., Edwards,S.J., Hananeia,L., Lasham,A., Royds,J., Sheard,P. and Braithwaite,A.W. (2003) Nuclear localization of Y-box factor YB1 requires wild-type p53. *Oncogene*, **22**, 2782–2794.
39. Gallouzi,I.E., Brennan,C.M., Stenberg,M.G., Swanson,M.S., Eversole,A., Maizels,N. and Steitz,J.A. (2000) HuR binding to cytoplasmic mRNA is perturbed by heat shock. *Proc. Natl. Acad. Sci. U.S.A.*, **97**, 3073–3078.
40. Kim,D., Pertea,G., Trapnell,C., Pimentel,H., Kelley,R. and Salzberg,S.L. (2013) TopHat2: accurate alignment of transcriptomes in the presence of insertions, deletions and gene fusions. *Genome Biol.*, **14**, R36.
41. Putri,G.H., Anders,S., Pyl,P.T., Pimanda,J.E. and Zanini,F. (2022) Analysing high-throughput sequencing data in Python with HTSeq 2.0. *Bioinformatics*, **38**, 2943–2945.
42. Sherman,B.T., Hao,M., Qiu,J., Jiao,X., Baseler,M.W., Lane,H.C., Imamichi,T. and Chang,W. (2022) DAVID: a web server for functional enrichment analysis and functional annotation of gene lists (2021update). *Nucleic Acids Res.*, **50**, 216–221.
43. Huang,da W., Sherman,B.T. and Lempicki,R.A. (2009) Systematic and integrative analysis of large gene lists using DAVID bioinformatics resources. *Nat. Protoc.*, **4**, 44–57.
44. Warde-Farley,D., Donaldson,S.L., Comes,O., Zuberi,K., Badrawi,R., Chao,P., Franz,M., Grouios,C., Kazi,F., Lopes,C.T. *et al.* (2010) The GeneMANIA prediction server: biological network integration for gene prioritization and predicting gene function. *Nucleic Acids Res.*, **38**, W214–W220.
45. Bailey,T.L., Johnson,J., Grant,C.E. and Noble,W.S. (2015) The MEME Suite. *Nucleic Acids Res.*, **43**, W39–W49.
46. Chen,X., Li,A., Sun,B.F., Yang,Y., Han,Y.N., Yuan,X., Chen,R.X., Wei,W.S., Liu,Y., Gao,C.C. *et al.* (2019) 5-methylcytosine promotes pathogenesis of bladder cancer through stabilizing mRNAs. *Nat. Cell Biol.*, **21**, 978–990.
47. Quinlan,A.R. and Hall,I.M. (2010) BEDTools: a flexible suite of utilities for comparing genomic features. *Bioinformatics*, **26**, 841–842.
48. Heinz,S., Benner,C., Spann,N., Bertolino,E., Lin,Y.C., Laslo,P., Cheng,J.X., Murre,C., Singh,H. and Glass,C.K. (2010) Simple combinations of lineage-determining transcription factors prime cis-regulatory elements required for macrophage and B cell identities. *Mol. Cell*, **38**, 576–589.
49. Remmert,M., Biegert,A., Hauser,A. and Söding,J. (2011) HHblits: lightning-fast iterative protein sequence searching by HMM-HMM alignment. *Nat. Methods*, **9**, 173–175.
50. Altschul,S.F., Madden,T.L., Schäffer,A.A., Zhang,J., Zhang,Z., Miller,W. and Lipman,D.J. (1997) Gapped BLAST and PSI-BLAST: a new generation of protein database search programs. *Nucleic Acids Res.*, **25**, 3389–3402.
51. Ko,J., Park,H., Heo,L. and Seok,C. (2012) GalaxyWEB server for protein structure prediction and refinement. *Nucleic Acids Res.*, **40**, W294–W297.
52. Söding,J., Biegert,A. and Lupas,A.N. (2005) The HHpred interactive server for protein homology detection and structure prediction. *Nucleic Acids Res.*, **33**, W244–W248.

53. Roy,A., Kucukural,A. and Zhang,Y. (2010) I-TASSER: a unified platform for automated protein structure and function prediction. *Nat. Protoc.*, **5**, 725–738.
54. Kelley,L.A., Mezulis,S., Yates,C.M., Wass,M.N. and Sternberg,M.J. (2015) The Phyre2 web portal for protein modeling, prediction and analysis. *Nat. Protoc.*, **10**, 845–858.
55. Chivian,D., Kim,D.E., Malmström,L., Bradley,P., Robertson,T., Murphy,P., Strauss,C.E., Bonneau,R., Rohl,C.A. and Baker,D. (2003) Automated prediction of CASP-5 structures using the Robetta server. *Proteins*, **53**, 524–533.
56. Kim,D.E., Chivian,D. and Baker,D. (2004) Protein structure prediction and analysis using the Robetta server. *Nucleic Acids Res.*, **32**, W526–W531.
57. Kim,D.E., Chivian,D., Malmström,L. and Baker,D. (2005) Automated prediction of domain boundaries in CASP6 targets using Ginzu and RosettaDOM. *Proteins*, **61**, 193–200.
58. Biasini,M., Bienert,S., Waterhouse,A., Arnold,K., Studer,G., Schmidt,T., Kiefer,F., Gallo Cassarino,T., Bertoni,M., Bordoli,L. *et al.* (2014) SWISS-MODEL: modelling protein tertiary and quaternary structure using evolutionary information. *Nucleic Acids Res.*, **42**, W252–W258.
59. Krieger,E., Joo,K., Lee,J., Lee,J., Raman,S., Thompson,J., Tyka,M., Baker,D. and Karplus,K. (2009) Improving physical realism, stereochemistry, and side-chain accuracy in homology modeling: four approaches that performed well in CASP8. *Proteins*, **77**, 114–122.
60. Holm,L. and Sander,C. (1992) Evaluation of protein models by atomic solvation preference. *J. Mol. Biol.*, **225**, 93–105.
61. Lovell,S.C., Davis,I.W., Arendall,W.B. 3rd, de Bakker,P.I., Word,J.M., Prisant,M.G., Richardson,J.S. and Richardson,D.C. (2003) Structure validation by Calpha geometry: phi,psi and Cbeta deviation. *Proteins*, **50**, 437–450.
62. Colovos,C. and Yeates,T.O. (1993) Verification of protein structures: patterns of nonbonded atomic interactions. *Protein Sci.*, **2**, 1511–1519.
63. Lüthy,R., Bowie,J.U. and Eisenberg,D. (1992) Assessment of protein models with three-dimensional profiles. *Nature*, **356**, 83–85.
64. Laskowski,R.A., Moss,D.S. and Thornton,J.M. (1993) Main-chain bond lengths and bond angles in protein structures. *J. Mol. Biol.*, **231**, 1049–1067.
65. Benkert,P., Biasini,M. and Schwede,T. (2011) Toward the estimation of the absolute quality of individual protein structure models. *Bioinformatics*, **27**, 343–350.
66. Ramírez-Aportela,E., López-Blanco,J.R. and Chacón,P. (2016) FRODOCK 2.0: fast protein-protein docking server. *Bioinformatics*, **32**, 2386–2388.
67. Park,T., Baek,M., Lee,H. and Seok,C. (2019) GalaxyTongDock: symmetric and asymmetric ab initio protein-protein docking web server with improved energy parameters. *J. Comput. Chem.*, **40**, 2413–2417.
68. Yan,Y., Tao,H., He,J. and Huang,S.Y. (2020) The HDOCK server for integrated protein-protein docking. *Nat. Protoc.*, **15**, 1829–1852.
69. Kozakov,D., Hall,D.R., Xia,B., Porter,K.A., Padhorny,D., Yueh,C., Beglov,D. and Vajda,S. (2017) The ClusPro web server for protein-protein docking. *Nat. Protoc.*, **12**, 255–278.
70. Schneidman-Duhovny,D., Inbar,Y., Nussinov,R. and Wolfson,H.J. (2005) PatchDock and SymmDock: servers for rigid and symmetric docking. *Nucleic Acids Res.*, **33**, W363–W367.
71. Torchala,M., Moal,I.H., Chaleil,R.A., Fernandez-Recio,J. and Bates,P.A. (2013) SwarmDock: a server for flexible protein-protein docking. *Bioinformatics*, **29**, 807–809.
72. Lyskov,S. and Gray,J.J. (2008) The RosettaDock server for local protein-protein docking. *Nucleic Acids Res.*, **36**, W233–W238.
73. Pettersen,E.F., Goddard,T.D., Huang,C.C., Couch,G.S., Greenblatt,D.M., Meng,E.C. and Ferrin,T.E. (2004) UCSF Chimera–a visualization system for exploratory research and analysis. *J. Comput. Chem.*, **25**, 1605–1612.
74. Watkins,A.M., Rangan,R. and Das,R. (2020) FARFAR2: improved de novo rosetta prediction of complex global RNA Folds. *Structure*, **28**, 963–976.
75. Sato,K., Kato,Y., Hamada,M., Akutsu,T. and Asai,K. (2011) IPknot: fast and accurate prediction of RNA secondary structures with pseudoknots using integer programming. *Bioinformatics*, **27**, i85–i93.
76. Yan,Y., Zhang,D., Zhou,P., Li,B. and Huang,S.Y. (2017) HDOCK: a web server for protein-protein and protein-DNA/RNA docking based on a hybrid strategy. *Nucleic. Acids. Res.*, **45**, W365–w373.
77. Kobayashi,S., Tanaka,T., Moue,M., Ohashi,S. and Nishikawa,T. (2015) YB-1 gene expression is kept constant during myocyte differentiation through replacement of different transcription factors and then falls gradually under the control of neural activity. *Int. J. Biochem. Cell Biol.*, **68**, 1–8.
78. Ohashi,S., Moue,M., Tanaka,T. and Kobayashi,S. (2011) Translational level of acetylcholine receptor alpha mRNA in mouse skeletal muscle is regulated by YB-1 in response to neural activity. *Biochem. Biophys. Res. Commun.*, **414**, 647–652.
79. Fujita,T., Ito,K., Izumi,H., Kimura,M., Sano,M., Nakagomi,H., Maeno,K., Hama,Y., Shingu,K., Tsuchiya,S. *et al.* (2005) Increased nuclear localization of transcription factor Y-box binding protein 1 accompanied by up-regulation of P-glycoprotein in breast cancer pretreated with paclitaxel. *Clin. Cancer Res.*, **11**, 8837–8844.
80. Miao,X., Wu,Y., Wang,Y., Zhu,X., Yin,H., He,Y., Li,C., Liu,Y., Lu,X., Chen,Y. *et al.* (2016) Y-box-binding protein-1 (YB-1) promotes cell proliferation, adhesion and drug resistance in diffuse large B-cell lymphoma. *Exp. Cell. Res.*, **346**, 157–166.
81. Luo,W., Chen,J., Li,L., Ren,X., Cheng,T., Lu,S., Lawal,R.A., Nie,Q., Zhang,X. and Hanotte,O. (2019) c-Myc inhibits myoblast differentiation and promotes myoblast proliferation and muscle fibre hypertrophy by regulating the expression of its target genes, miRNAs and lincRNAs. *Cell Death Differ.*, **26**, 426–442.
82. Miner,J.H. and Wold,B.J. (1991) c-myc inhibition of MyoD and myogenin-initiated myogenic differentiation. *Mol. Cell. Biol.*, **11**, 2842–2851.
83. Kim,H.H., Kuwano,Y., Srikantan,S., Lee,E.K., Martindale,J.L. and Gorospe,M. (2009) HuR recruits let-7/RISC to repress c-Myc expression. *Genes Dev.*, **23**, 1743–1748.